NASA CR-172,477

NASA Contractor Report 1724-77

Data Appendix:

F-Number = 1.0 EMR With A Flexible Back Electrode

D.J. Mihora
Technical Staff

GENERAL RESEARCH CORPORATION

Contract NAS1-16133
August 1984

National Aeronautics and
Space Administration

Langley Research Center
Hampton, Virginia 23665

CONTENTS

FIGURES

Figures (Continued)

TABLES

1 INTRODUCTION

NASA, Langley Research Center has recently completed testing a low f-number Electrostatic Membrane Reflector, (EMR) in Hampton, Virginia. The initial report on this test effort was documented in NASA CR-165792, dated June 29, 1981. This technical report will present the test data which was obtained on 8 to 14 May 1984 on this model. The test data is sparse--only three sets of measurements were taken on this configuration. Lack of funds at NASA has halted the present testing of this configuration. Ordinarily, initial test data on this type of antenna are used for a preliminary alignment and adjustment of this adaptive structure to an improved figure. However, in this austere program, the design improvements suggested by the test data could not be exercised. Only the three initial calibration runs are available for review in this report.

The antenna reflector being measured was designed[1] to achieve a spherical reflector surface with a focal length to diameter ratio (f_n) of one and a potential accuracy of 1.0 mm over its 4.88 m diameter. The configuration required the cutting and joining of twelve pie-shaped panels to form the reflector surface. Electrostatic forces are used to tension this preformed membrane reflector. The design details of this configuration were prescribed by NASA.

During this program, NASA fabricated four membrane reflector surfaces, one from Mylar[2] and Kapton[3] and two from Tedlar.[4] Each membrane reflector had a somewhat different preformed shape. Kapton is a "space qualified" material and exhibits very low creep. Tedlar has a low hygroscopic and thermal expansion coefficient. NASA decided to use

---

[1] D.J. Mihora, Preliminary Design Notes on a Low F-Number EMR, NASA CR-165953, May 1982.

[2] Dupont Trademark, PET, Polyethylene Terephthalate

[3] Dupont Trademark, PPMI, Polypyromelitimide (polyimide)

[4] Dupont Trademark, PVF, Polyvinylfluoride

12.5 m (0.5 mil) Tedlar for the membrane reflector.

Ten independent high-voltage power supplies were incorporated into the design. These power supplies as well as the rim support structure were acquired from the prior successful $f_N = 3.5$ EMR program.

The test results to be presented here are very poor. The measured shape of the membrane surface is far removed from the desired shape. Several obvious design corrections are required for the configuration to realize the expected figure. The design corrections are described in this document. At the top of the recommendations is a higher level of quality control in the manufacturing of the preformed membranes. Next, the proper electrostatic force distribution must be generated, which will necessitate higher sustained voltages on the outermost eight electrodes. A detailed discussion of these and other design recommendations is presented in Sec. 4.

The contents of this data report are as follows: Sec. 2 describes the baseline design including photos of the EMR during testing. The test data is presented in Sec. 3 including 3-D plots which readily illustrate the problems. Recommendations for design improvements are contained in Sec. 4. Finally, Sec. 5 provides a derivation of the gore geometry for the f_n 1.0 membrane reflector.

Use of trademarks or names of manufacturers in this report does not constitute an official endorsement of such products or manufacturers, either expressed or implied, by the National Aeronautics and Space Administration.

2 CONFIGURATION

The configuration being evaluated is an axisymmetric reflector with potential applications for mm and cm-wave radars and radiometers. The reflector surface is a thin conducting membrane. The membranes are aluminized polymer films with thicknesses of 7.5 to 12.5 μm (0.3 to 0.5 mil).

The present design is axisymmetric with a diameter of 488 cm. The concept is very unconventional. It utilizes electrostatic forces to tension and adjust the shape of the reflector membrane.

In schematic view, the EMR appears very analogous to actively controlled glass mirrors. Depicted in Figure 2.1 is the tension stiffened membrane (the primary concave aperture), the actuators or control segments which are driven by the control voltages V, a microprocessor, and finally the figure sensor. Most of the technology being developed for the active control of flexible structures is applicable to this concept. In some ways the EMR is easier to model and simulate because it is a continuous surface rather than multiple surfaces. There are indeed many similarities to flexible, controlled glass mirrors and there are also major differences which will be highlighted in this section.

The electrostatic membrane reflector is essentially a large area capacitor with one of the capacitor electrodes being the membrane reflector surface. It is a thin, deformable, shape-adjustable surface. When a voltage is applied between this reflector surface and the other electrode or multiple electrodes shown in Fig. 2.1, the electrostatic attractive force (Coulomb's force) draws the thin membrane inward. The thin membrane can be formed into different concave shapes. It is possible to form smooth surfaces such as spheres, parabolas, and ellipsoids. It is difficult to introduce wavy or high spatial frequency surfaces with electrostatics.

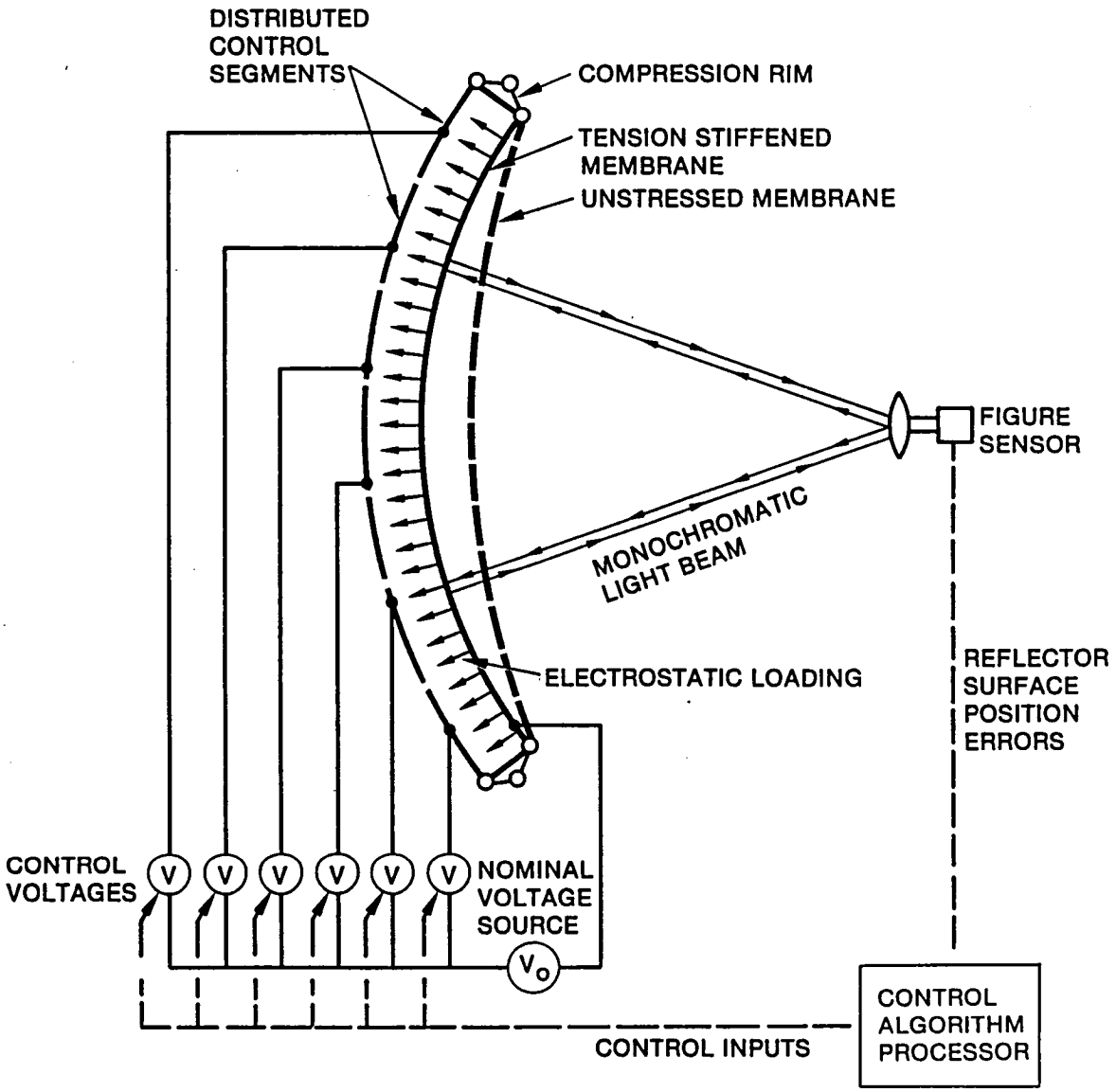

Figure 2.1 Electrostatic Membrane Reflector (EMR) Conceptual View

The electrostatic forces that form and maintain the surface are limited in magnitude by corona or breakdown of the electric field between the plates. In air, an electric field strength E_e of 800 kV/m (20 kV/in) can be successfully implemented provided some care is maintained in the layout. The electrostatic pressure felt on the membrane is $P = \varepsilon_o E_e^2/2$ where $\varepsilon_o = 8.84 \times 10^{-12}$ F/m is the free space dielectric constant. The nominal electrostatic pressure P in air is about 2.6 N/m^2 (0.05 lb/ft^2). This pressure is small by one measure, atmospheric pressure being about 10^5 N/m^2. However, it is many orders of magnitude larger than solar pressure. Using lightweight membranes (thickness h = 7 - 15μm) this force can produce stresses of 5 to 10 percent of yield. Since the magnitude of electrostatic force is a constraint in air tests, thin membranes are dictated. The thin membranes predispose the EMR to be extremely light.

At the heart of the EMR is the thin, electrically conducting membrane which is tensioned and controlled by the pressure field. This membrane conductor is a ground surface of the configuration. For a spherical membrane, the centerline stress is $\sigma = \rho P/2h$

where $P \leq 2.8$ N/m^2

$h = 7$ μm (reflector thickness)

$\rho = 9.76$ m, radius of curvature (for this example)

The resulting stress in the membrane is nominally 1.9×10^6 N/m^2 (283 lb/in^2) which is more than adequate to produce relatively "stiff" structure.

The membrane reflector requires a spatially and temporally controllable pressure field on the membrane. Spatial control is achieved by segmenting the back control electrode as portrayed in Fig.

2.1. Each electrode element is electrically isolated from the neighbor element. Each of these elements can be adjusted in voltage relative to the ground (membrane reflector). Each of these elements can thus exert a different field strength and pressure on the nearby membrane. Like pneumatic pressure, the electrostatic pressure is applied normal to the (conducting) membrane; but unlike penumatic pressure, the electrostatic pressure can be altered very rapidly. Small changes in applied force produce linear changes in deflection. For example, a 200 V change in electrode voltage results in a 1.0 μm deflection of the membrane over the control electrode.

In summary, the EMR appears very attractive because:

(1) The pressure is controllable with voltage changes to a very high temporal frequency.

(2) Micro-weight solid-state power supplies can be used.

(3) Transistor-transistor logic (TTL) controlled high voltage power supplies can be an integral part of a closed-loop control system.

(4) There are no moving mechanical parts other than the actual membrane reflector.

2.1 4.88m f_n-3.5 mm-WAVE REFLECTOR

The original EMR of a reasonably large size is shown in Figs. 2.2 and 2.3. The two figures contrast the initially flat (and wrinkled) Kapton membrane and the subsequent electrostatically tensioned EMR. This configuration was designed in 1979, fabricated at NASA, Langley Research Center, Virginia, and tested in 1980-1981. The components, including the membrane reflector, are commercially available items. (The program was also completed under a very austere budget.) The 16-foot aperture diameter represented a size that was not too large to handle manually but not too small to obtain data over a reasonable area. It was decided that an axisymmetric surface had many advantages for a preliminary model. One such advantage was the simplicity of the control electrodes (actuators) which were 5 annular rings. The membrane reflector and the circular rim attachment were the electrical ground

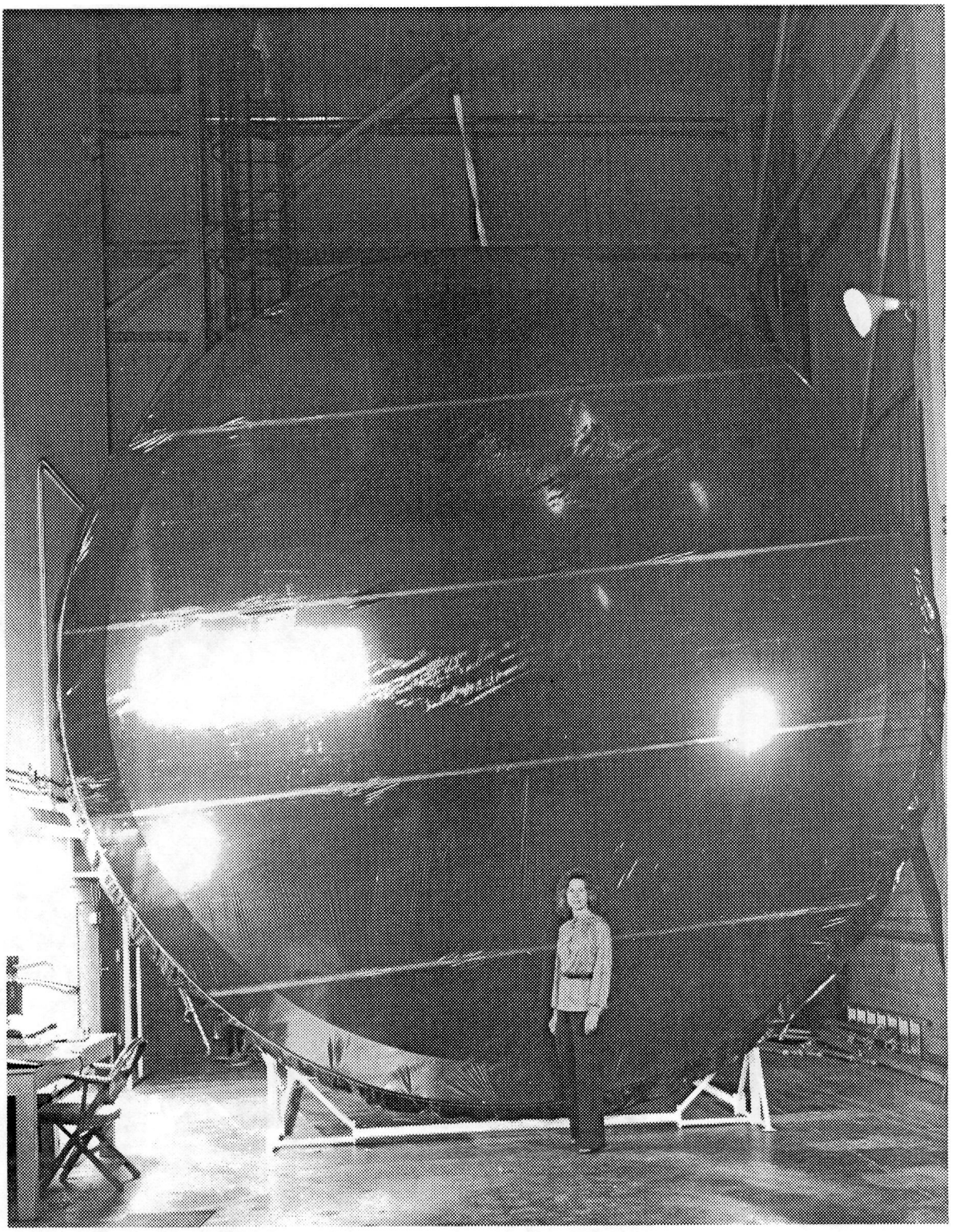

Figure 2.2 EMR Without Applied Voltage Shown
to Illustrate the "Striations" in the Commercial Polymer Film

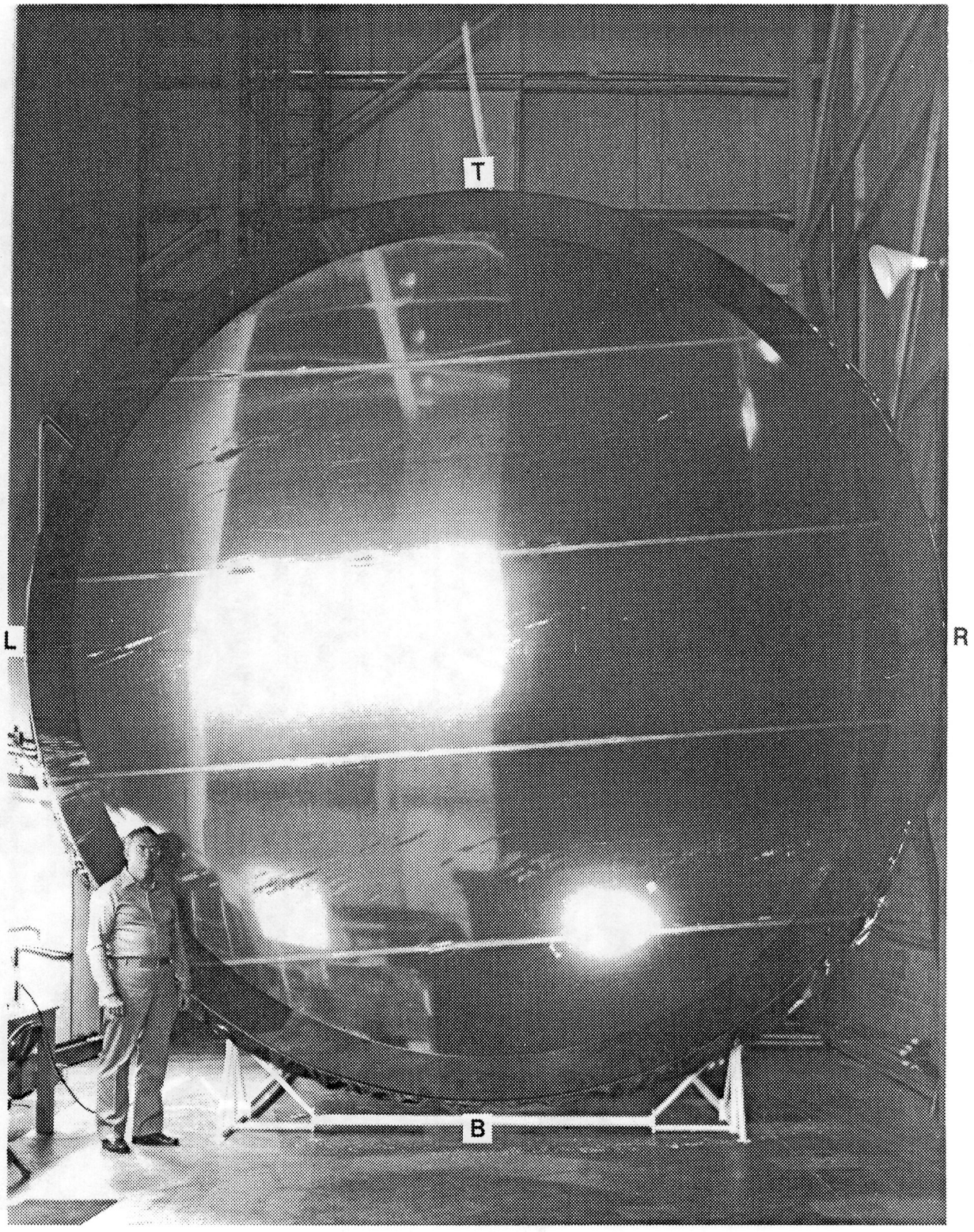

Figure 2.3 EMR With the Application of 45 kV Potential to Form a f_n 3.5 Spherical mm-wave Reflector From a Flat Kapton Membrane

reference for the high voltage power supplies. The width of each of the five flat control electrodes shown in Fig. 2.4 was selected to provide best shape control when deforming the flat (untensioned) membrane surface to a tensioned sphere.

Readily available 0.3 and 0.5 mil Kapton, 0.5 mil Mylar, and 0.5 mil polyethylene were used in four different tests. The wrinkles seen in Fig. 2.2 appear to be typical of those present in the commercial grade of Kapton. Commercial Mylar is much smoother, but the material is significantly orthotropic. The membrane shown in Figs. 2.2 and 2.3 is aluminized Kapton with the aluminized side facing the control electrodes and the diffuse Kapton surface facing the camera. Four seams are evident. The seams provide a practical test of fabricating and manufacturing large membrane reflector surfaces. The radius of curvature for this model is quite large. It is 34 meters. When forming this radius of curvature, the membrane center point moves about 87 mm (3.4 in). This deflection was adequate to induce a stress that is about 6 percent of yield stress (626 psi) in the membrane reflector which visually eliminated most wrinkles and imperfections. The f-number of 3.5 is larger than desirable for full-scale reflectors, but provided a good initial test bed for experimentation. A low f-number configuration requires a preformed membrane reflector. The current configuration is a low f-number design and its attributes will be discussed next.

2.2 CURRENT CONFIGURATION

The data and analysis of this report concerns the low f-number EMR which incorporates a preformed, curved membrane reflector. This configuration is a substantial modification of the $f_N = 3.5$ EMR built in 1979. The present configuration has a 4.88 m diameter and exhibits an f-number of approximately 1.0.

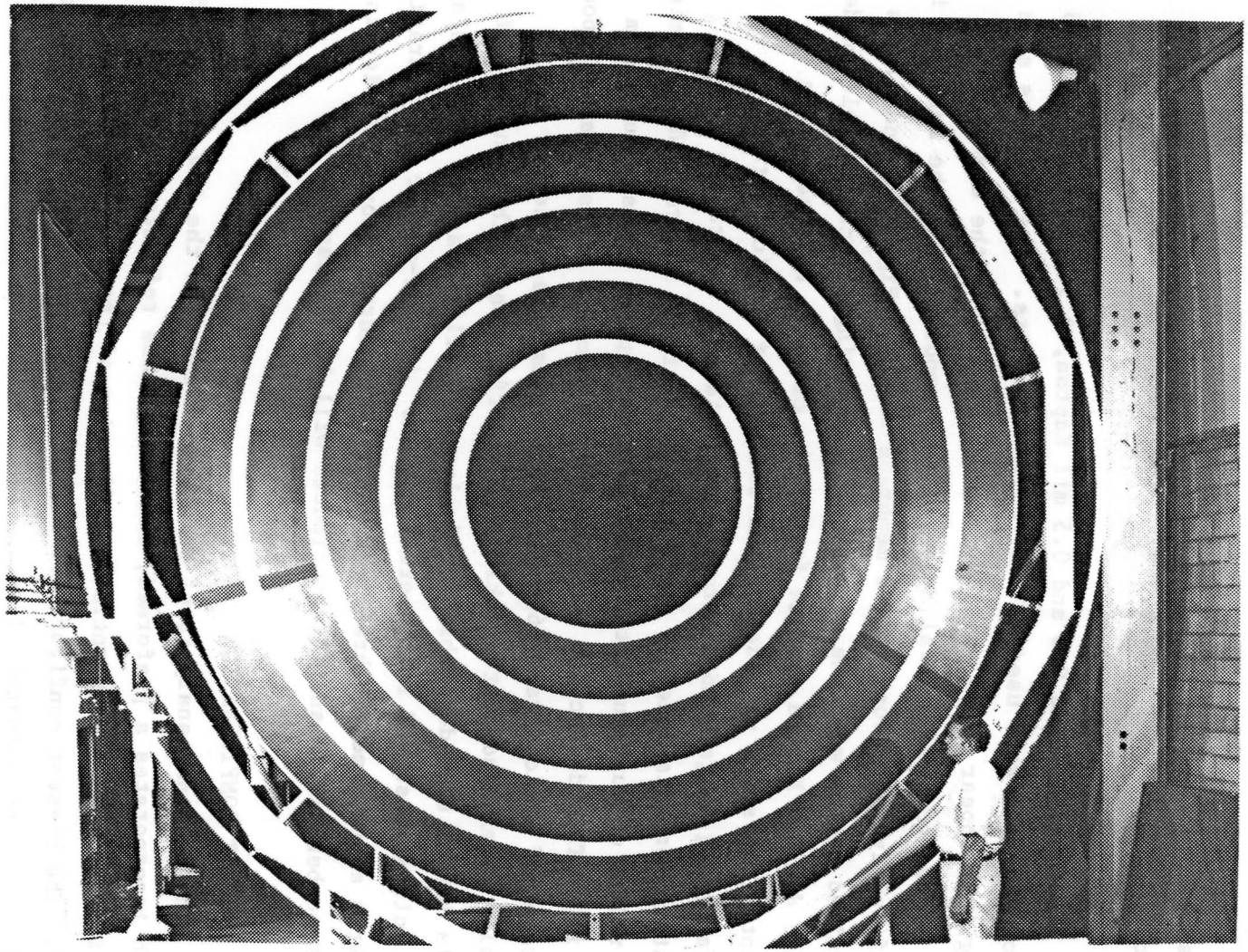

Figure 2.4 Annular Control Electrodes on the f_n 3.5 EMR

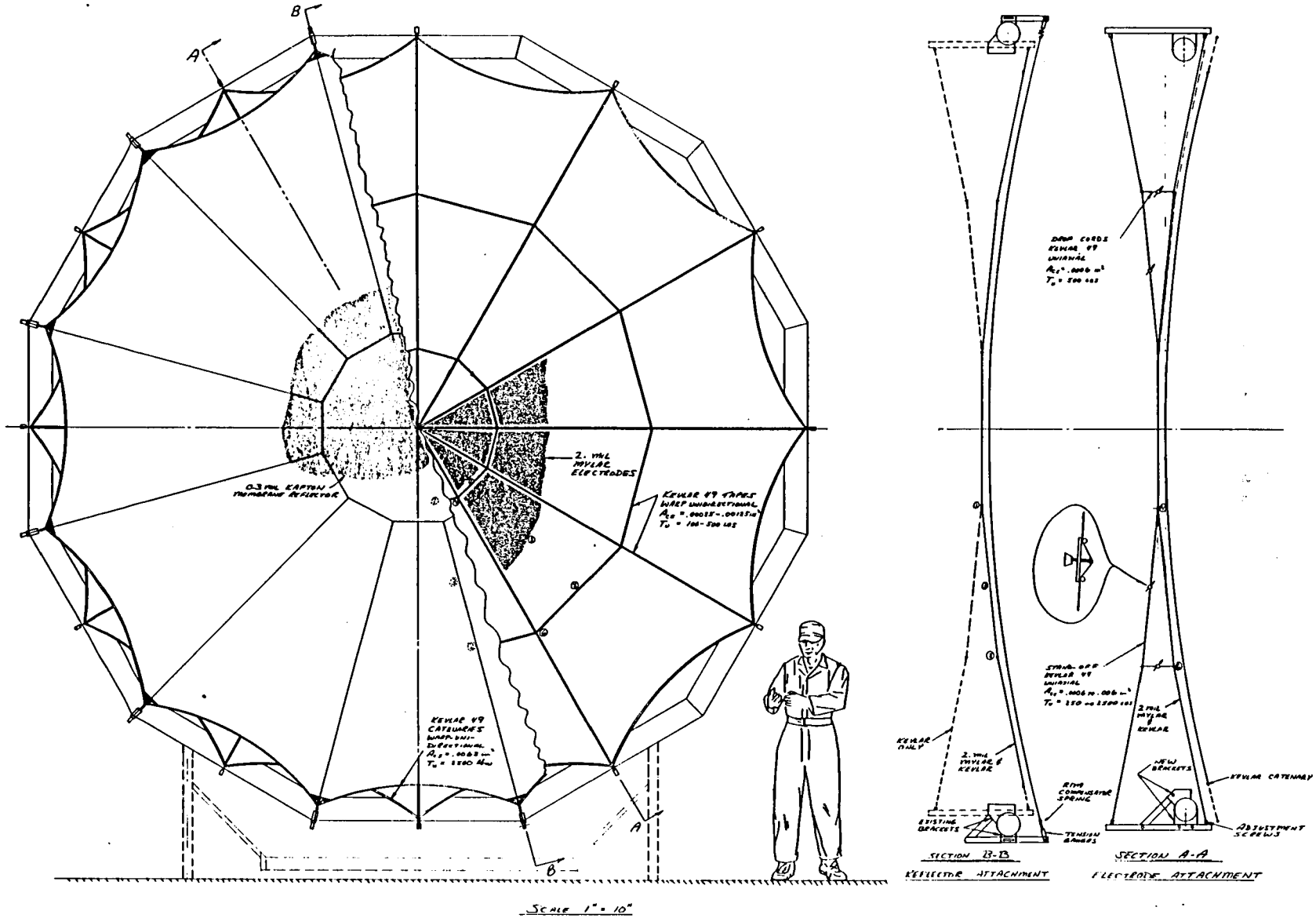

Scale 1" = 10"

Figure 2.5 Flexible Electrode EMR--1982 Design
(Modification of the 1979 Testbed)

To achieve a low f-number requires the fabrication of a preformed membrane. Because this is a "shoestring" activity at NASA and at GRC, the available funds required fabrication from materials on hand, which included Mylar, Kapton and Tedlar film on rolls. The membrane material could only be curved in one direction. Thus, there are flat panels or straight lines rather than curved arcs in parts of the preformed aperture. Twelve pie-shaped panels were used in the fabrication of the reflector surface. Figure 2.5 shows the front and two sectional views of the membrane reflector and the electrode surface. The electrode surface was also formed using flat sheet material into an approximate spherical shape. This configuration makes maximum use of existing test equipment. The same rim structure, power supplies, and measurement systems that were used on the 1979 ($f_N = 3.5$) design were retained for this ($f_N = 1$) design.

Ten power supplies are used to adjust the membrane shape. Azimuthal control along the perimeter will incorporate 8 of the 10 power supplies. The nominal electrostatic pressure is 2.6 $N/^2$ (0.05 lb/ft^2) generated with an electric field strength of 7.7 kV/cm (19.5 kV/in). It was expected that a surface quality of about 1 mm might be achieved with this design. The main limitation on surface quality is the membrane material and the quality control in layup and fabrication of this deepdish. Probably the most challenging fabrication task is the catenary layup onto the membrane reflector.

NASA has informed GRC that four membrane reflector surfaces were fabricated during this program. Only the last fabricated sample is discussed in this report. All four reflector surfaces were constructed on a narrow seam template. Costs prevented fabrication on a complete master mold of the full aperture. Twelve gore panels of flat membrane film were spliced together to construct the following four surfaces:

Sample 1: A Langley Research Center (LARC) gore template (derived from a meteorological balloon) was used as a template for 0.5 mil Mylar. The formed surface apparently exhibited excessive concavity near the perimeter. This surface was modified by reducing the gore width nearly 1/4 inch near the perimeter. This new gore shape apparently yielded a better surface. The centerline deflection was 12.8 in.

Sample 2: A Kapton membrane 0.3 mil thick was fabricated using the sample gore pattern used with Sample 1. An accident with this membrane prevented data from being acquired.

Sample 3: A Tedlar membrane 0.5 mil thick was constructed using the same gore pattern used in Sample 1. The data in this report pertains to this configuration.

Sample 4: A Tedlar membrane 0.5 mil thick was constructed using the gore shape described in Sec. 5. No test data is available on this sample.

A front view of the membrane reflector in the untensioned state is shown in Figure 2.6. The twelve pie shaped gores are evident despite the numerous azimuthal creases. The influence of gravity on this surface is not evident. The application of electrostatic force to this membrane will only eliminate a fraction of the wrinkles. Unfortunately, this preformed membrane shape was not close to the desired preformed spherical shape. Figure 2.7 shows the membrane reflector partially tensioned. A higher stress or electrostatic force was not available. A contamination of the insulator region between electrodes limited the applied voltage to values below the desired 32 kV potential on the eight outermost electrodes. It is not apparent from Figure 2.7 but the center portion of the membrane has deflected approximately 28 cm with the application of electrostatic force.

Figure 2.6 Twelve Gore Tedlar Surface

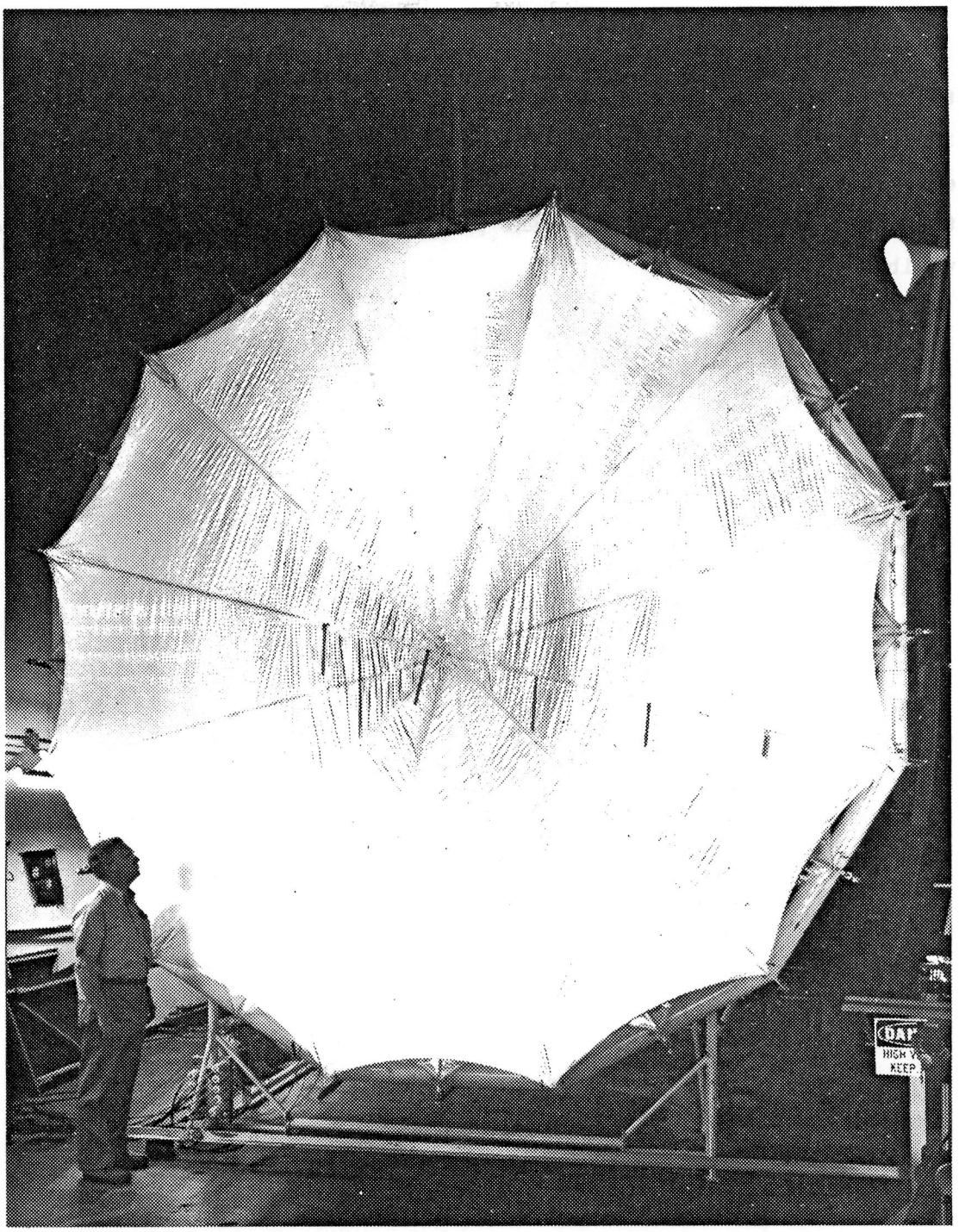

Figure 2.7 Tedlar Partially Tensioned With Electrostatics

The centerline deflection of the membrane is more apparent from the edge views of Fig. 2.8 vs. Fig. 2.9. In Fig. 2.8 the membrane is influenced by gravity forces. In Fig. 2.9 the membrane is tensioned by electrostatic forces. The sketch to the right of each photo identifies the lines visible in the adjacent photo. The gore seam lines are barely visible in Fig. 2.9.

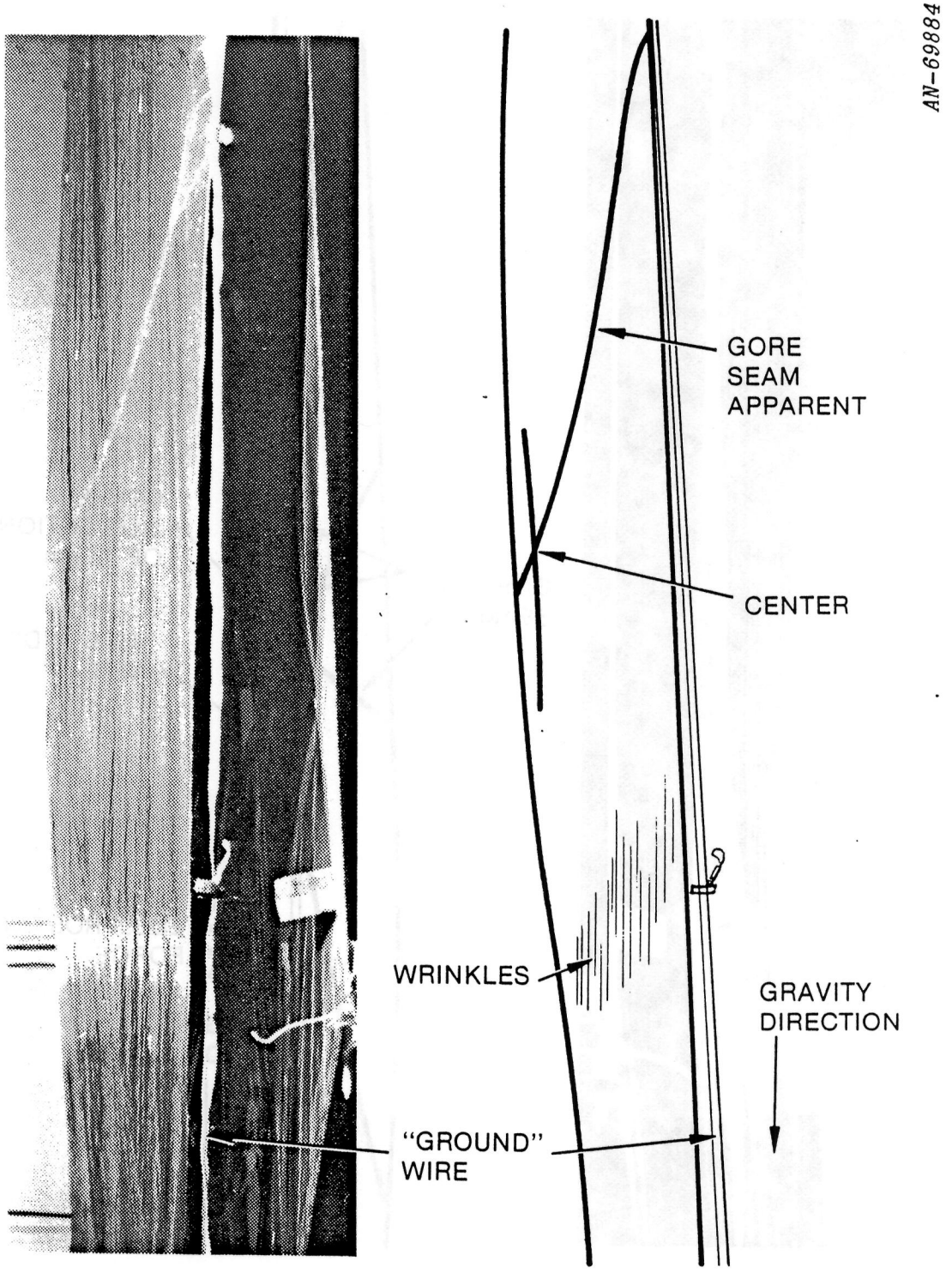

Figure 2.8 Edge View of Tedlar Membrane Acted On by Gravity

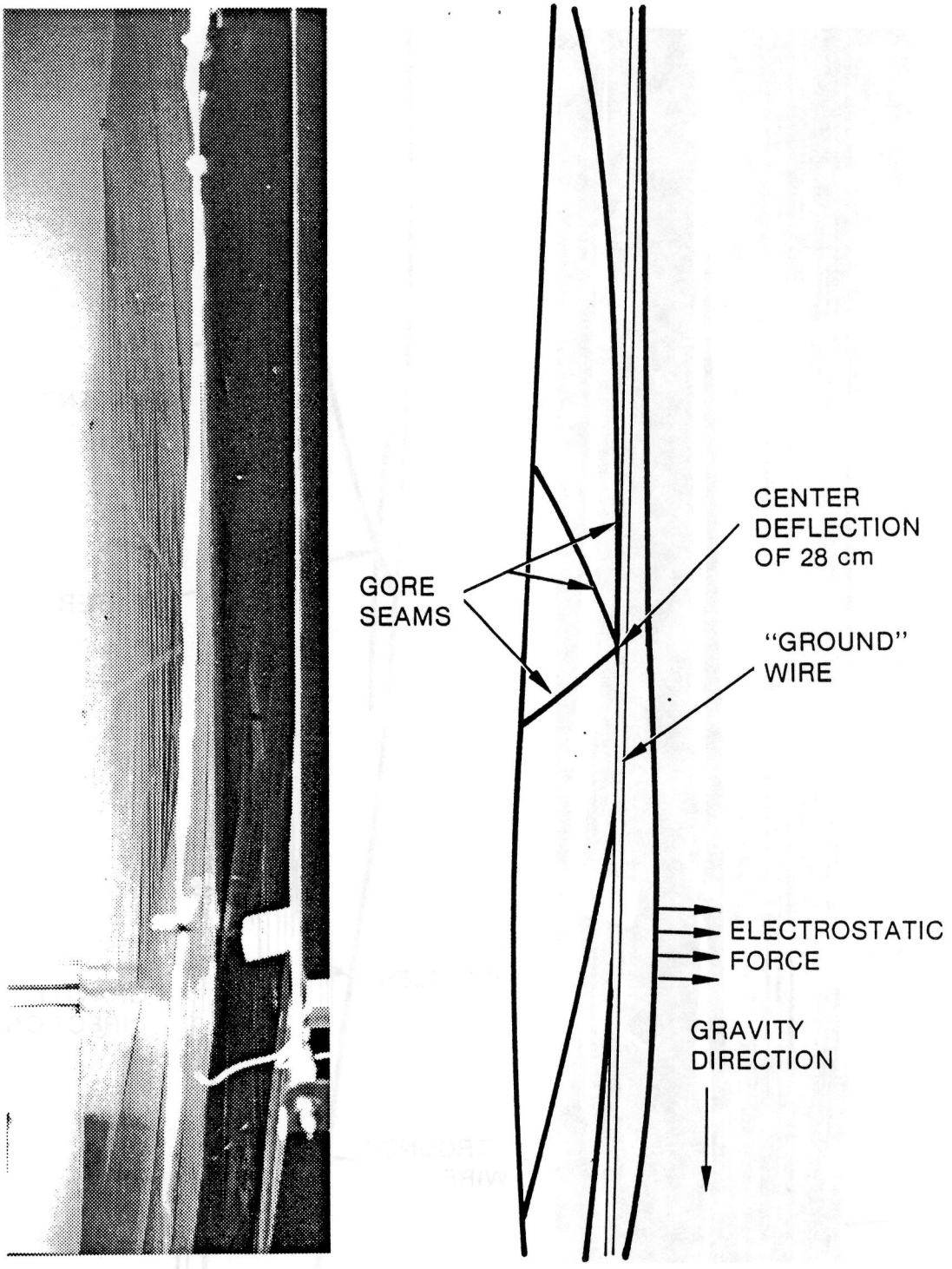

Figure 2.9 Edge View of Tedlar Membrane Partially Tensioned with Electrostatics

3 TEST DATA

Three sets of test measurements were made on the Tedlar membrane. In each set, 73 target points on the membrane surface were measured using two K & E theodolites. Approximately two hours are required to manually aim the theodolites and acquire the necessary output data. Fig. 3.1 indicates the relative location of the 73 target points. Points 1 thru 12 are located at the apex of the catenaries. Points 202, 206 and 210 are located on the mounting brackets which retain the electrode surface. These three points are used to define a reference-plane when presenting the 73 membrane reflector displacements. The circled numbers in Fig. 3.1 refer to the ten electrode regions located behind the membrane reflector.

The three sets of test measurements are designated GOS100, GOS80, and GOS60 to denote 100, 80, and 60 percent of available working voltage. An important test, GOS100 was an attempt to maximize the electrical field strength. The limitation was a corona or a high sustained current leading to premature discharge of the outer eight electrodes. The electrostatic force was only about 80 percent of the design requirement. This reduced loading state was well below prior tests.

Unfortunately, tests at higher membrane stress levels like those achieved in the f_N 3.5 design (Fig. 2.3) were not possible with this f_N 1.0 configuration.

Premature discharge of the outermost electrodes during test GOS100 has been partially attributed to contamination at the insulator region between the electrodes. Apparently, conductive paint accidentally seeped into small seams of the electrode surface during fabrication. These seams are located at the insulator gap region between the electrodes. The conductive paint provides current flow to ground which precipitated premature discharges.

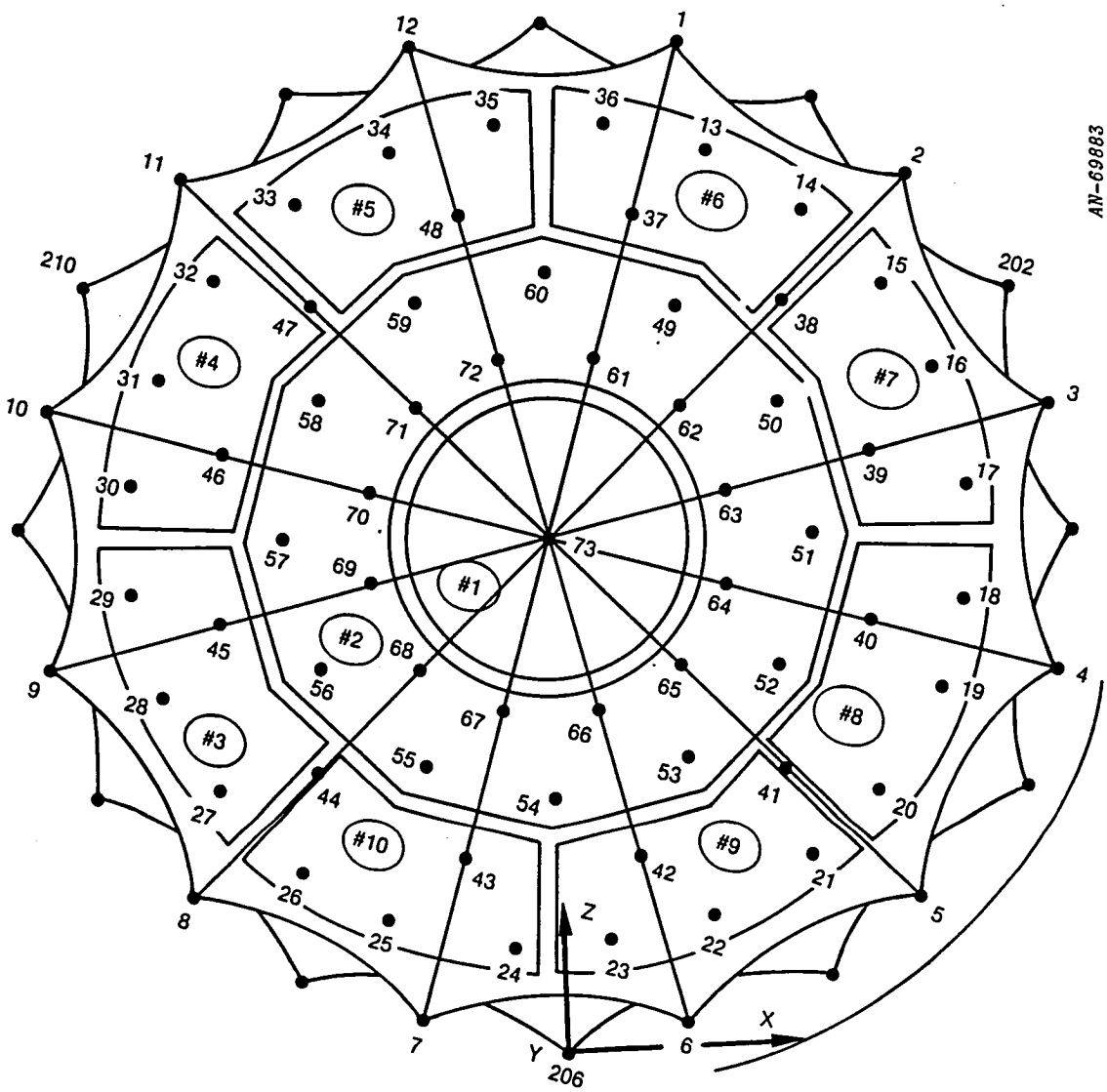

Figure 3.1 Location of Measurement Points on EMR

Note: Another cause of the current leakage could have been an adhesive which was used as "sizing" for the Mylar surface before the conductive paint was applied.

Unfortunately, the adhesive which was left in the insulator region between electrodes may have also contaminated the insulator gap.

The two tests at 60 and 80 percent of maximum sustained voltage provide force vs. deflection data at reduced membrane stress.

Tables 3.1 thru 3.3 present the test data in the form used for subsequent data plotting. The x, y, z coordinate location is shown in Fig. 3.1. The tabular data is presented in the following format:

Column 1: Point number
Column 2: x-coordinate (ft), horizontal
Column 3: y-coordinate (ft) deflection relative to the x-z plane. The x-z plane is a local theodolite reference plane.
Column 4: z-coordinate (ft), vertical
Column 5: y-coordinate (in), is the membrane deflection relative to the x-z plane and is defined as that which minimizes the RMS errors through the rim points 1 thru 12.

3.1 3-D SHAPES BY PROJECTION

A very illustrative method of portraying the test results has used 3-D projections of the surface errors. The 3-D projections provide a visual reconstruction of the propagation of anomalies over the reflector. This visual reconstruction of the test data was useful in a prior test program[1] with the $f_N = 3.5$ aperture. Improvements made after visualizing the errors had led to an order of magnitude improvement in overall quality. In this austere program, only one set of data was taken. Unfortunately, the financial constraints prevented retesting with design improvements.

[1] D.J. Mihora, Test Progress on the Electrostatic Membrane Reflector, NASA CR-165792, June 1981.

Table 3.1

TEST DATA GOS-100 - MAXIMUM VOLTAGES ON 5-7-84

N	X (ft)	Y (ft)	Z (ft)	Y (in)
1	2.19682	-0.09793	16.56413	0.08880
2	5.95982	-0.06003	14.43723	0.02114
3	8.10587	-0.04272	10.69037	-0.03888
4	8.10007	-0.05309	6.36735	-0.11126
5	5.94292	-0.06009	2.64264	0.16291
6	2.20704	-0.13043	0.47594	-0.11184
7	-2.11131	-0.17853	0.47337	-0.06061
8	-5.84571	-0.22197	2.64381	-0.06416
9	-8.00492	-0.23405	6.40037	0.06054
10	-7.99805	-0.22787	10.71064	0.08261
11	-5.83458	-0.21540	14.43562	-0.12682
12	-2.09858	-0.14924	16.61455	0.09753
13	2.59242	0.14482	14.73091	2.96577
14	4.13997	0.14402	13.82223	2.74175
15	5.33674	0.14951	12.62188	2.64768
16	6.22157	0.16127	11.06336	2.67856
17	6.66282	0.17221	9.42955	2.76503
18	6.65949	0.20071	7.63487	3.12872
19	6.22135	0.23070	5.99876	3.57169
20	5.32096	0.23518	4.44544	3.77497
21	4.11877	0.17490	3.24359	3.24085
22	2.57005	0.15190	2.35087	3.20077
23	0.93624	0.12897	1.90728	3.16873
24	-0.85570	0.13121	1.90510	3.45636
25	-2.49267	0.09106	2.34680	3.20757
26	-4.04209	0.07678	3.24824	3.25098
27	-5.24773	0.06695	4.45610	3.29410
28	-6.14475	0.07254	6.01465	3.47320
29	-6.58956	0.04480	7.66118	3.18558
30	-6.57979	0.04596	9.45615	3.17679
31	-6.13916	0.05014	11.08773	3.14350
32	-5.23000	0.05529	12.64256	3.05447
33	-4.03026	0.06683	13.84283	3.00416
34	-2.47357	0.10485	14.73845	3.22323
35	-0.83598	0.14354	15.17475	3.44402
36	0.95814	0.18485	15.16855	3.67863
37	1.33144	0.40770	13.33762	6.32013
38	3.54511	0.38333	12.04523	5.72083
39	4.81676	0.37284	9.81960	5.43631
40	4.81739	0.40472	7.25632	5.84918
41	3.53257	0.39306	5.03395	5.92257
42	1.31533	0.37420	3.74827	6.03427
43	-1.24709	0.36314	3.74844	6.27435
44	-3.45369	0.31344	5.03779	5.98383
45	-4.03026	0.29422	7.27212	5.91251
46	-4.72418	0.27736	9.82761	5.67891

Table 3.1

(CONTINUED)

N	X (ft.)	Y (ft.)	Z (ft.)	Y (in)
47	-3.43853	0.28417	12.03851	5.54739
48	-1.22351	0.36220	13.32110	6.14606
49	1.89007	0.54354	11.79252	7.88706
50	3.26074	0.51321	10.42355	7.33997
51	3.76515	0.50403	8.56306	7.17843
52	3.27102	0.51855	6.68842	7.44684
53	1.91766	0.51760	5.31014	7.64874
54	0.05233	0.54627	4.79316	8.27027
55	-1.80849	0.50850	5.28505	8.08209
56	-3.18833	0.47105	6.65497	7.81720
57	-3.69864	0.44131	8.52673	7.51239
58	-3.20002	0.43711	10.39167	7.36737
59	-1.83793	0.47691	11.76945	7.63029
60	0.03316	0.55649	12.28421	8.30683
61	0.67597	0.68493	10.94057	9.77041
62	1.78508	0.66695	10.29569	9.40093
63	2.41730	0.63508	9.18076	8.93979
64	2.41402	0.62321	7.89949	8.81302
65	1.77290	0.64162	6.78694	9.14038
66	0.67150	0.67616	6.14557	9.72273
67	-0.60564	0.66837	6.14594	9.81509
68	-1.70319	0.62403	6.78947	9.43516
69	-2.33442	0.58245	7.90373	9.01489
70	-2.33462	0.57558	9.17834	8.91726
71	-1.69798	0.61063	10.28438	9.23215
72	-0.59750	0.67449	10.92022	9.83065
73	0.03005	0.78906	8.54257	11.14232

TABLE 3.2

TEST DATA GOS80-80 PERCENT VOLTAGES ON 5-10-84

N	X (ft.)	Y (ft.)	Z (ft.)	Y (in)
1	2.19998	-0.10784	16.56337	0.02848
2	5.96194	-0.06392	14.43639	0.03007
3	8.10768	-0.04442	10.68871	-0.00634
4	8.10066	-0.05770	6.36479	-0.11478
5	5.94165	-0.06198	2.64006	0.19262
6	2.20555	-0.13280	0.47478	-0.08575
7	-2.11055	-0.18486	0.47276	-0.07932
8	-5.84504	-0.22586	2.64241	-0.05036
9	-8.00432	-0.24047	6.39909	0.04668
10	-7.99718	-0.23222	10.71036	0.09474
11	-5.83274	-0.22061	14.43630	-0.12548
12	-2.09614	-0.15674	16.61414	0.06943
13	2.59505	0.11717	14.72847	2.69191
14	4.14145	0.11655	13.82080	2.46878
15	5.33751	0.12165	12.62107	2.36907
16	6.22136	0.12435	11.06181	2.29026
17	6.66213	0.13897	9.42789	2.42003
18	6.65770	0.16803	7.63273	2.79015
19	6.21918	0.19918	5.99714	3.24700
20	5.32174	0.21125	4.44512	3.54100
21	4.12250	0.16988	3.24098	3.23378
22	2.56817	0.15055	2.34788	3.23948
23	0.93525	0.12793	1.90393	3.21202
24	-0.85654	0.12360	1.90368	3.42196
25	-2.49146	0.07528	2.34570	3.07617
26	-4.03909	0.04266	3.24898	2.90061
27	-5.24209	0.01118	4.45740	2.68481
28	-6.13801	0.01883	6.01477	2.88964
29	-6.58314	-0.00450	7.66129	2.65573
30	-6.57494	0.00986	9.45418	2.80608
31	-6.13446	0.01451	11.08407	2.77866
32	-5.22467	0.01176	12.63756	2.59470
33	-4.02599	0.01916	13.83725	2.49424
34	-2.47039	0.05546	14.73206	2.69207
35	-0.83403	0.08293	15.16639	2.77741
36	0.96023	0.11621	15.15892	2.91442
37	1.33283	0.33715	13.32946	5.53215
38	3.54582	0.32198	12.03986	5.04152
39	4.81630	0.31554	9.81564	4.80422
40	4.81492	0.35669	7.25391	5.32777
41	3.53233	0.36818	5.03149	5.67885
42	1.31696	0.36947	3.74516	6.03308
43	-1.24501	0.34036	3.74705	6.05837
44	-3.44882	0.27421	5.03731	5.57203
45	-4.72434	0.24486	7.27169	5.38049
46	-4.71701	0.23252	9.82696	5.20184

TABLE 3.2

(CONTINUED)

N	X (ft.)	Y (ft.)	Z (ft.)	Y (in)
47	-3.43360	0.24329	12.03678	5.11786
48	-1.22008	0.30656	13.31594	5.53859
49	1.89191	0.47809	11.78693	7.15938
50	3.26085	0.44704	10.41948	6.60256
51	3.76260	0.44111	8.56042	6.47944
52	3.26999	0.47063	6.68613	6.92735
53	1.91782	0.48969	5.30805	7.36977
54	0.05347	0.52053	4.79214	8.01838
55	-1.80477	0.47207	5.28464	7.70287
56	-3.18304	0.42119	6.65408	7.27810
57	-3.69332	0.39069	8.52598	6.96508
58	-3.19619	0.38191	10.38929	6.76552
59	-1.83314	0.41761	11.76541	6.97862
60	0.03679	0.48859	12.27827	7.55100
61	0.67911	0.60891	10.93515	8.91630
62	1.78529	0.60070	10.29127	8.66359
63	2.41742	0.57238	9.17724	8.24411
64	2.41266	0.56237	7.89652	8.13953
65	1.77342	0.59280	6.78537	8.61104
66	0.67252	0.63316	6.14502	9.26368
67	-0.60404	0.61644	6.14636	9.24968
68	-1.70029	0.57014	6.78880	8.84703
69	-2.33105	0.52249	7.90252	8.35464
70	-2.33141	0.51511	9.17614	8.25140
71	-1.69451	0.54412	10.28126	8.49357
72	-0.59374	0.59901	10.91419	8.98386
73	0.03257	0.72117	8.54030	10.38555

TABLE 3.3

TEST DATA GOS60-60 PERCENT ON 5-10-85

N	X (ft.)	Y (ft.)	Z (ft.)	Y (in)
1	2.19904	-0.11895	16.56293	-0.05403
2	5.96214	-0.06825	14.43646	0.03632
3	8.10756	-0.04710	10.68871	0.02771
4	8.10125	-0.06122	6.36386	-0.08486
5	5.94114	-0.06734	2.63857	0.20313
6	2.20414	-0.13949	0.47374	-0.09292
7	-2.11151	-0.19355	0.47278	-0.11611
8	-5.84585	-0.22817	2.64190	-0.01825
9	-8.00474	-0.24273	6.39873	0.07128
10	-7.99799	-0.23570	10.70987	0.09880
11	-5.83386	-0.22604	14.43524	-0.14724
12	-2.09698	-0.15994	16.61515	0.07607
13	2.59414	0.07684	14.72668	2.26173
14	4.14019	0.07152	13.81831	1.98557
15	5.33622	0.07557	12.61872	1.87628
16	6.21917	0.07869	11.06009	1.80601
17	6.65871	0.09201	9.42679	1.92322
18	6.65431	0.12068	7.63263	2.29108
19	6.21426	0.14364	5.99804	2.65161
20	5.31822	0.16561	4.44601	3.06521
21	4.11938	0.14002	3.24171	2.94750
22	2.56754	0.13346	2.34737	3.10529
23	0.93436	0.11649	1.90299	3.14412
24	-0.85657	0.10373	1.90381	3.25055
25	-2.49116	0.05805	2.34567	2.93364
26	-4.03831	0.02216	3.25006	2.71555
27	-5.24214	0.00444	4.45706	2.66178
28	-6.13874	0.01205	6.01450	2.86294
29	-6.58379	-0.01884	7.65966	2.53547
30	-6.57246	-0.01878	9.45320	2.51133
31	-6.13082	-0.02075	11.08296	2.40253
32	-5.22212	-0.02427	12.63622	2.20855
33	-4.02517	-0.01171	13.83435	2.17025
34	-2.46707	0.02033	14.73032	2.31720
35	-0.83273	0.04675	15.16358	2.39177
36	0.96087	0.08358	15.15863	2.57371
37	1.33319	0.28506	13.32752	4.96102
38	3.54310	0.27164	12.03770	4.49643
39	4.81312	0.26601	9.81526	4.27358
40	4.81157	0.30412	7.25472	4.76428
41	3.52807	0.32017	5.03293	5.17157
42	1.31440	0.33812	3.74624	5.72457
43	-1.24683	0.30747	3.74782	5.72801
44	-3.44940	0.24900	5.03812	5.32893
45	-4.72569	0.21958	7.27050	5.13203
46	-4.71746	0.19146	9.82476	4.76035

TABLE 3.3

(CONTINUED)

N	X (ft.)	Y (ft.)	Z (ft.)	Y (in)
47	-3.43334	0.19685	12.03402	4.61029
48	-1.21865	0.25972	13.31190	5.02714
49	1.88882	0.42703	11.78446	6.60398
50	3.25644	0.40035	10.41821	6.10336
51	3.75745	0.39023	8.56064	5.93337
52	3.26623	0.42060	6.68709	6.39317
53	1.91523	0.44746	5.30931	6.92921
54	0.05167	0.48094	4.79429	7.60774
55	-1.80565	0.43397	5.28605	7.30695
56	-3.18389	0.39150	6.65441	6.97945
57	-3.69369	0.35404	8.52439	6.57958
58	-3.19446	0.33034	10.38713	6.19873
59	-1.83323	0.35998	11.76006	6.33930
60	0.03659	0.42508	12.27266	6.84275
61	0.67734	0.53611	10.93089	8.09955
62	1.78177	0.53576	10.28825	7.94364
63	2.41522	0.51738	9.17576	7.64563
64	2.40986	0.51132	7.89614	7.59028
65	1.77118	0.54275	6.78530	8.07431
66	0.67087	0.58355	6.14603	8.73164
67	-0.60420	0.56361	6.14742	8.67717
68	-1.70027	0.52621	6.78869	8.37896
69	-2.33174	0.48316	7.90134	7.93960
70	-2.33056	0.46603	9.17384	7.71736
71	-1.69433	0.48410	10.27697	7.82776
72	-0.59247	0.52826	10.90904	8.18966
73	0.03271	0.67523	8.54082	9.89321

Usually, the graphical portrayal of the measured surface is in the form of an error distribution. The error distribution is generated by subtracting the measured shape from the ideal (spherical) shape. The expectation was that the magnitude of the error distribution would be less than 1.0 mm (RMS). Unfortunately, this first series of tests did not come anywhere close to the original goals. The errors measured in these initial tests are so substantial that they can be identified from the direct shape projections. The subsequent discussion will present both the direct shape measurements and the error distributions for three tests.

The voltages used in the three tests in May 1984 are summarized in Table 3.4. The three tests did not match the voltages or central deflection of the ideal design layout. Two major difficulties developed. First, the desired voltage potential could not be achieved in the outer 8 electrodes which comprise 53 percent of the overall electrode surface area. Premature discharge of the outer electrodes prevented testing to design levels. One probable reason for the discharge of the perimeter electrodes is contamination. NASA indicated that conductive paint was inadvertently left in small cracks when the Mylar electrode surface was fabricated. Also, "sizing" used on the surface of Mylar apparently created surface paths for the voltage feed-over. A second difficulty involved the shape of the preformed surface. Apparently, an improper gore pattern or lack of an accurate master mold led to a preformed surface that was not close to the desired spherical surface. The differences in the fabricated reflector as compared to the designed reflector layout were very substantial. It will be shown that the manufactured model is far from the desired spherical shape and electrostatics cannot compensate for these substantial errors.

The shape of the membrane reflector from test GOS100 is shown in Fig. 3.2. This case has the largest voltage potential of the three test

Table 3.4

VOLTAGE DISTRIBUTIONS FOR MAY 1984 TESTS

Test	ΔZ (m)	V_1(kV) centerline	V_2 (kV) first ring	V_3 thru V_{10} perimeter ring	% Loading
Ideal Layout	.3099	38.7	36.5	32.0 thru 32.0	1.0
GOS100	.283	52.	42.	23, 26, 25, 26, 30, 23, 26, 25	.98
GOS80	.264	42.	33.	20. thru 20.	.608
GOS60	.251	31.	25	14. thru 14.	.32

cases. The surface appears in form to be an inverted cone. The twelve catenary attachment points are located relative to the reference plane which minimizes rim out-of-plane errors. This reflector surface is closer in shape to a cone rather than the desired spherical shape. The desired spherical surface shown in Fig. 3.3 provides a dramatic contrast to the measured surface. The spherical surface in Fig. 3.3 has a radius of curvature of 10.65 m. This curvature is the approximate average of the measured surface in Fig. 3.2.

The poor membrane shape in Fig. 3.2 is attributed to several factors. The dominant error source appears to be the manufactured shape which is not replicating the desired 9.85 m, preformed spherical curvature. A second factor could be an excessive radial force applied during the set-up and alignment of the catenaries. An excessive radial force at the apex of each catenary will tend to deform the preformed sphere into more of a conic shape. A third detrimental effect is the applied voltage potential which applies an excessive pressure near the apex and a very diminished pressure near the perimeter. The pressure is proportional to voltage squared. Notice in Table 3.4 that the voltages of the three tests are not in agreement with the prescribed layout. Specifically, the prescribed layout dictated a centerline to perimeter voltage ratio, $V_1/V_{10} = 38.7/32 = 1.2$ and pressure ratio of 2.105. In the tests, the centerline to perimeter voltage ratio was 2.1 to 2.2 and the pressure ratio was 3.1 to 3.4. Thus, the pressure at the centerline was excessively large. All three of the previously discussed factors influenced the shape in a detrimental way yielding a "conical" surface rather than the desired "spherical" surface.

The distribution of surface errors for test GOS100 is shown in Fig. 3.4. The error distribution is simply the measured shape (Fig. 3.2) minus the ideal shape (Fig. 3.3). The dominant error is the axisymmetric shape difference between the two surfaces. The localized or gore to gore waviness is smaller than the difference between the

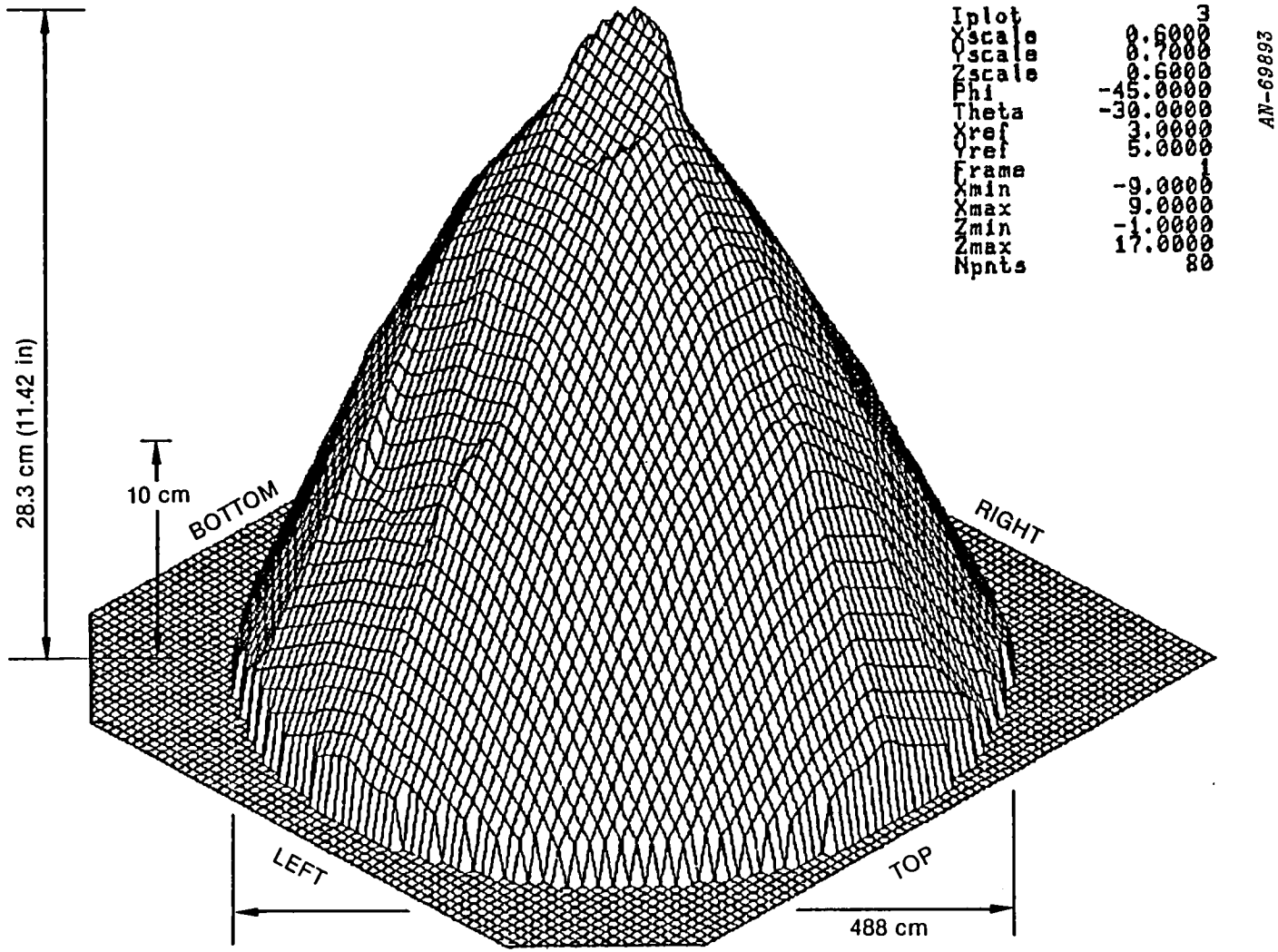

Figure 3.2 Measured Reflector Shape From Test GOS100

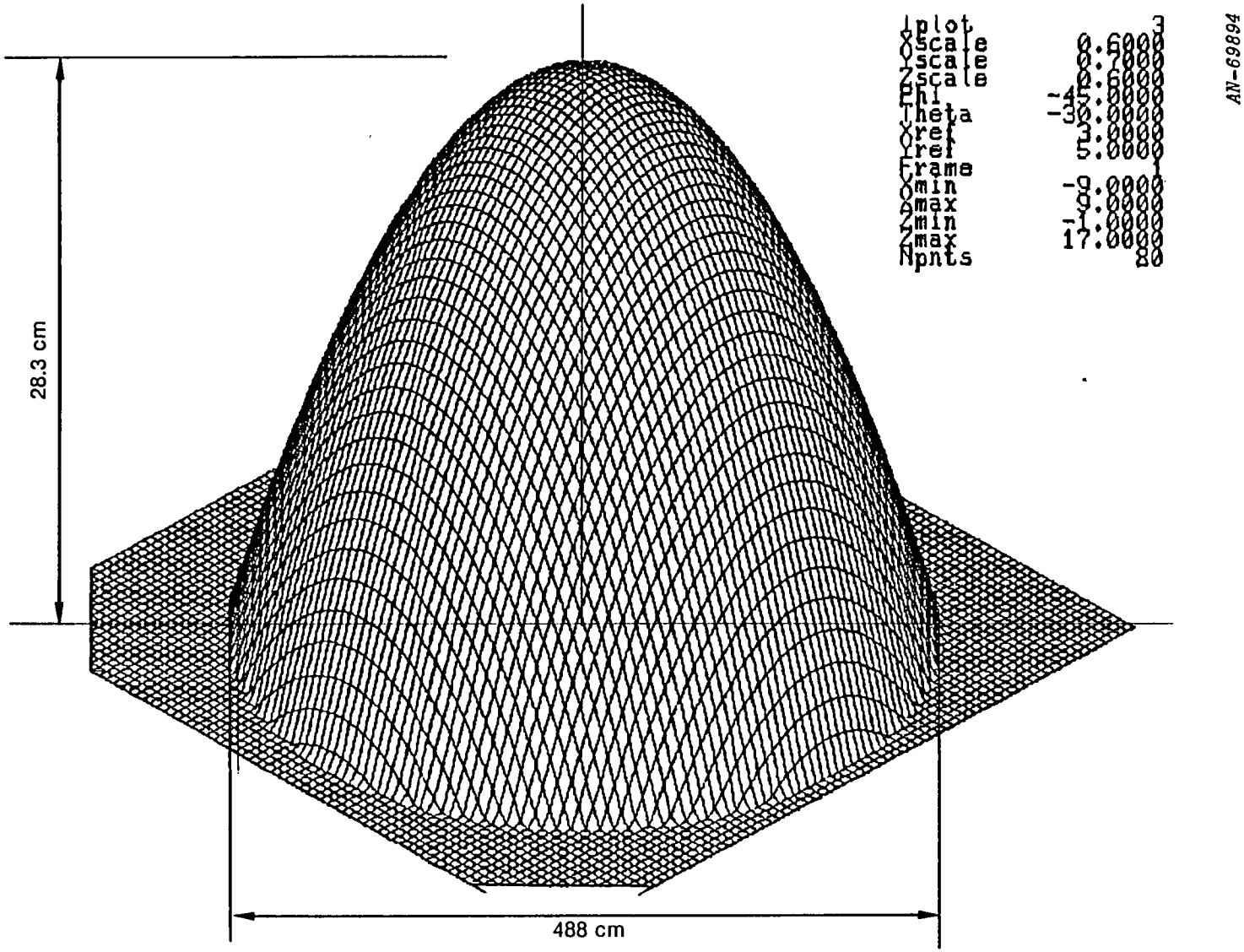

Figure 3.3 Ideal Reflector Shape -- Curvature 10.65 m

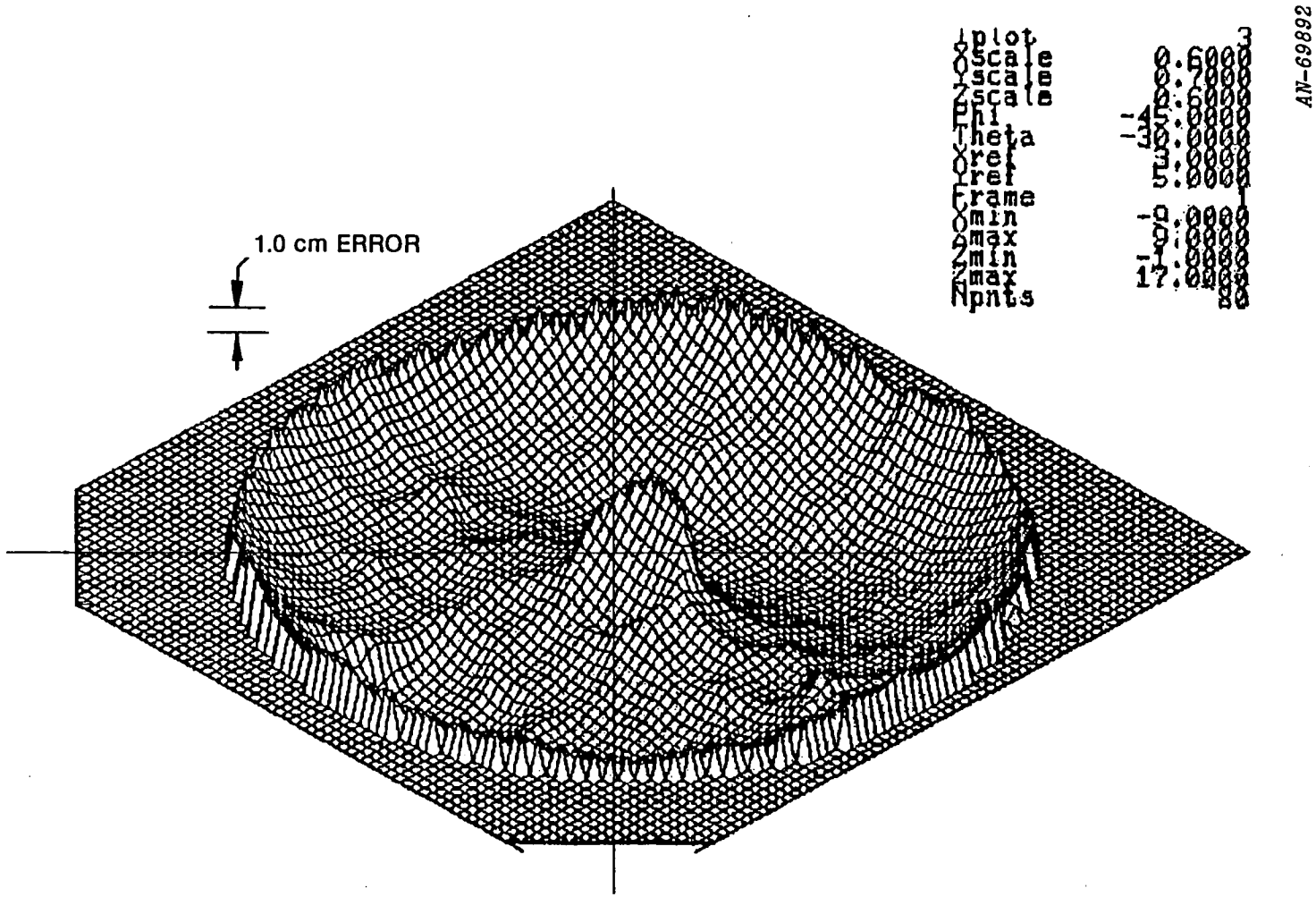

Figure 3.4 Surface Error Distribution for Test GOS100
(Ideal Curvature - 10.65m)

conical (test) and spherical (ideal) shapes. A vertical reference scale of 1.0 cm is shown in Fig. 3.4. The largest error is about 2.5 cm and the RMS error is about 1.2 cm.

Additional views of the error distributions are shown in Figs. 3.5 and 3.6. The difference is the view angle. In Fig. 3.5, the left face of the aperture is in the foreground while in Fig. 3.6 the top of the aperture is in the foreground. Figures 3.4 thru 3.6 indicate the dominant error is axisymmetric—i.e. the formed shape is not a sphere but is more nearly a conic.

Two tests were performed at reduced voltage potentials of 80 and 60 percent of the values used in test GOS100. The purpose of these tests were to assess the influence of electrostatics on the preformed shape. At these reduced potentials, the stresses and forces are 64 and 36 percent of the baseline case. The reduced forces and deflections allow an estimate of the preformed membrane shape without electrostatics. This estimate is important because a direct measurement of the preformed shape is unavailable with the rim in a vertical plane. A direct measurement of the preformed shape requires the rim to be in the horizontal plane. Shape measurements in the horizontal orientation were unavailable since a relocating of the theodolite measurement system could not be achieved in the short time span of the tests. The measurements at the reduced pressures were adequate to assess the quality of the preformed surfaces.

The formed membrane shapes at the lower voltage potentials are very similar to the maximum potential case. The conical unformed shape is evident in all three tests, the main difference being the reduced deflection at the centerline. As indicated in Table 3.4, the centerline deflection is reduced by a factor of 0.887 between the highest potential test, GOS100, and the lowest potential test, GOS60. The retention of the conical shape at low forces indicates that the preformed shape is not the desired preformed sphere.

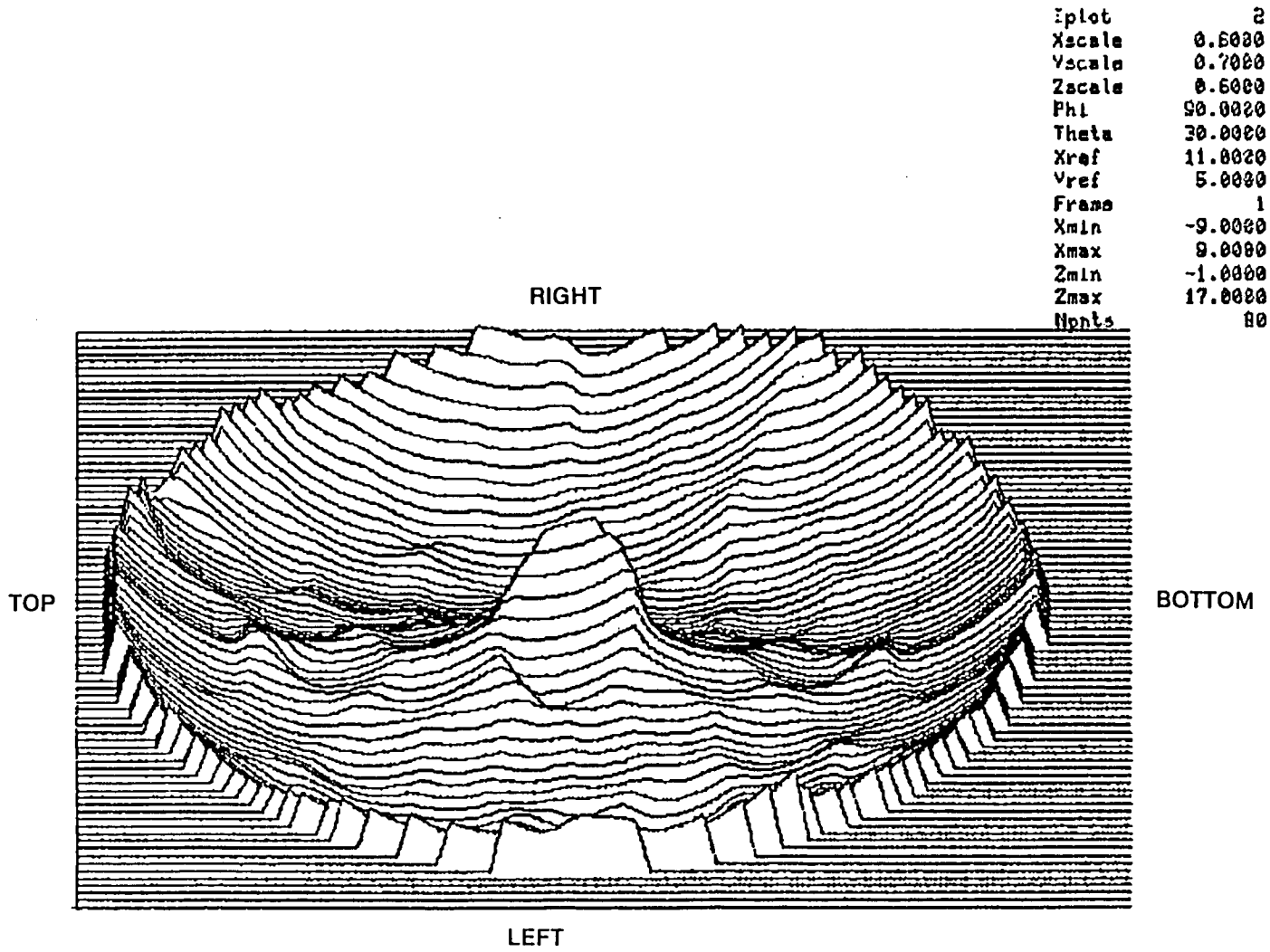

Figure 3.5 Side View of Surface Error Distribution for Test GOS100

Iplot	1
Xscale	0.6000
Yscale	0.7000
Zscale	0.6000
Phi	0.0000
Theta	-30.0000
Xref	6.0000
Yref	7.0000
Frame	1
Xmin	-9.0000
Xmax	9.0000
Zmin	-1.0000
Zmax	17.0000
Npnts	80

AN-69887

BOTTOM

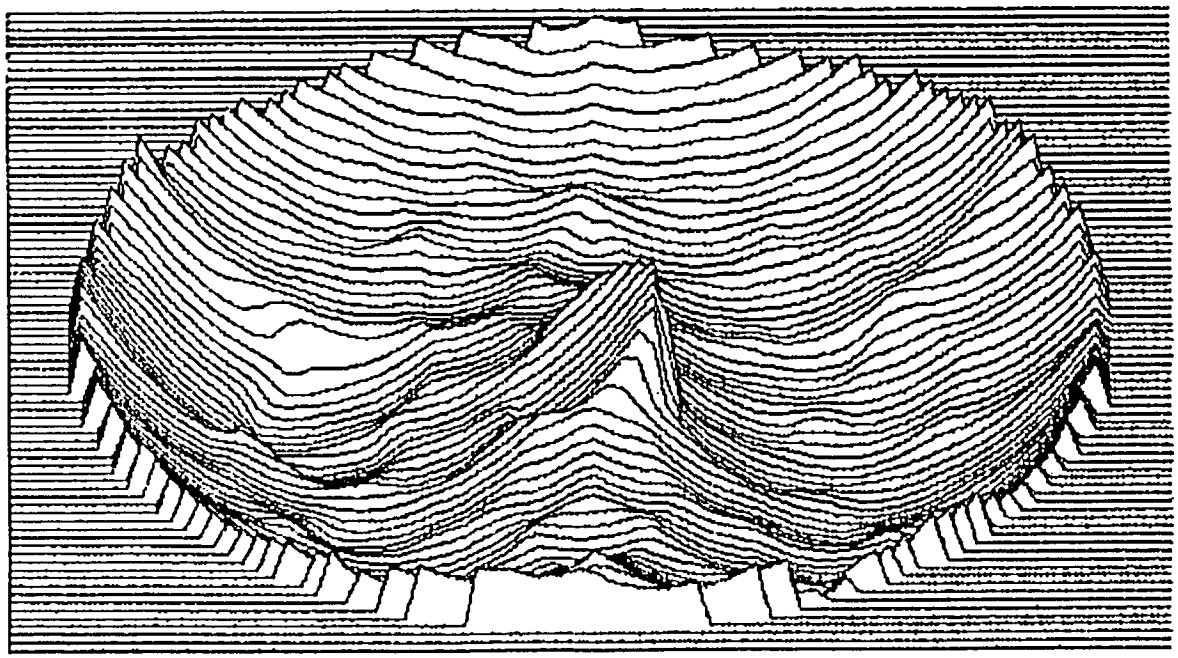

LEFT

RIGHT

TOP

Figure 3.6 Top View of Surface Error Distribution
For Test GOS100

The measured conical shape of test G0S80 is shown in Fig. 3.7. The centerline sag is 26.37 cm as compared to the 28.3 cm for the full potential case. This shape is nearly identical to the original shape presented in Fig. 3.2. The error distribution for the G0S80 test is shown in Fig. 3.8. The vertical scale is the measured surface minus the (ideal) spherical surface with an 11.4 m curvature. This curvature is the average value of the measured shape. The error distribution in Fig. 3.8 is nearly identical to the error distribution in Fig. 3.4.

The third test case, G0S60, is shown in Figs. 3.9 and 3.10. The shape and error distribution are also very similar to the two prior examples. The average curvature for this third test case was 11.96 m.

Table 3.5 summarizes the results for the three tests. Included in this table is the centerline deflection, Δz, the maximum excursion from the ideal shape Z_m, the average curvature ρ, and the RMS error σ_Z from the ideal spherical surface. The largest deviation and RMS errors are attributed to the improper preformed shape. An encouraging aspect of the test results is the lower magnitude of the ripples and distortions caused by the laminating of the 12 gore segments.

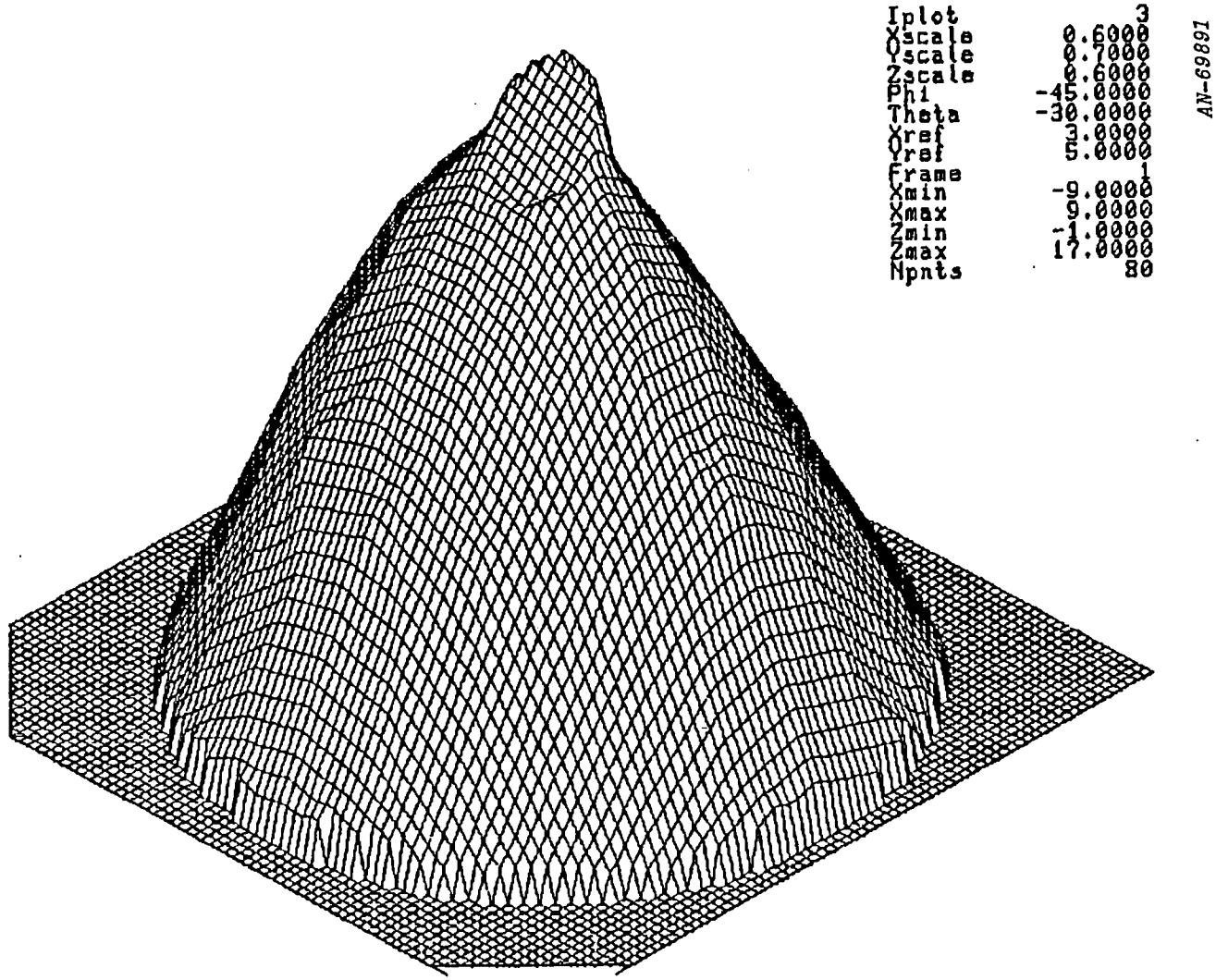

Figure 3.7 Measured Reflector Shape From Test GOS80

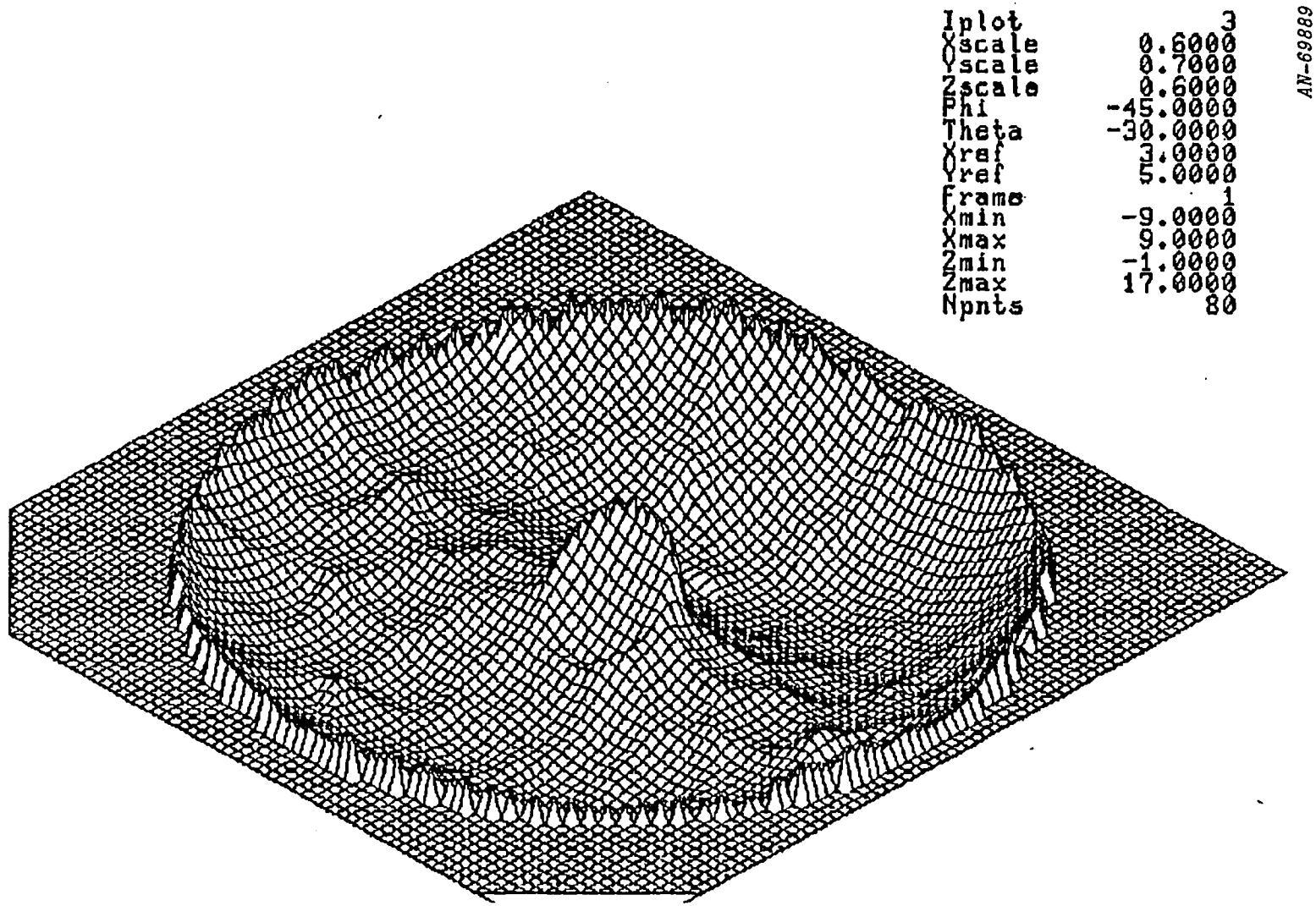

Figure 3.8 Surface Error Distribution for Test GOS80
(Ideal Curvature = 11.4 m)

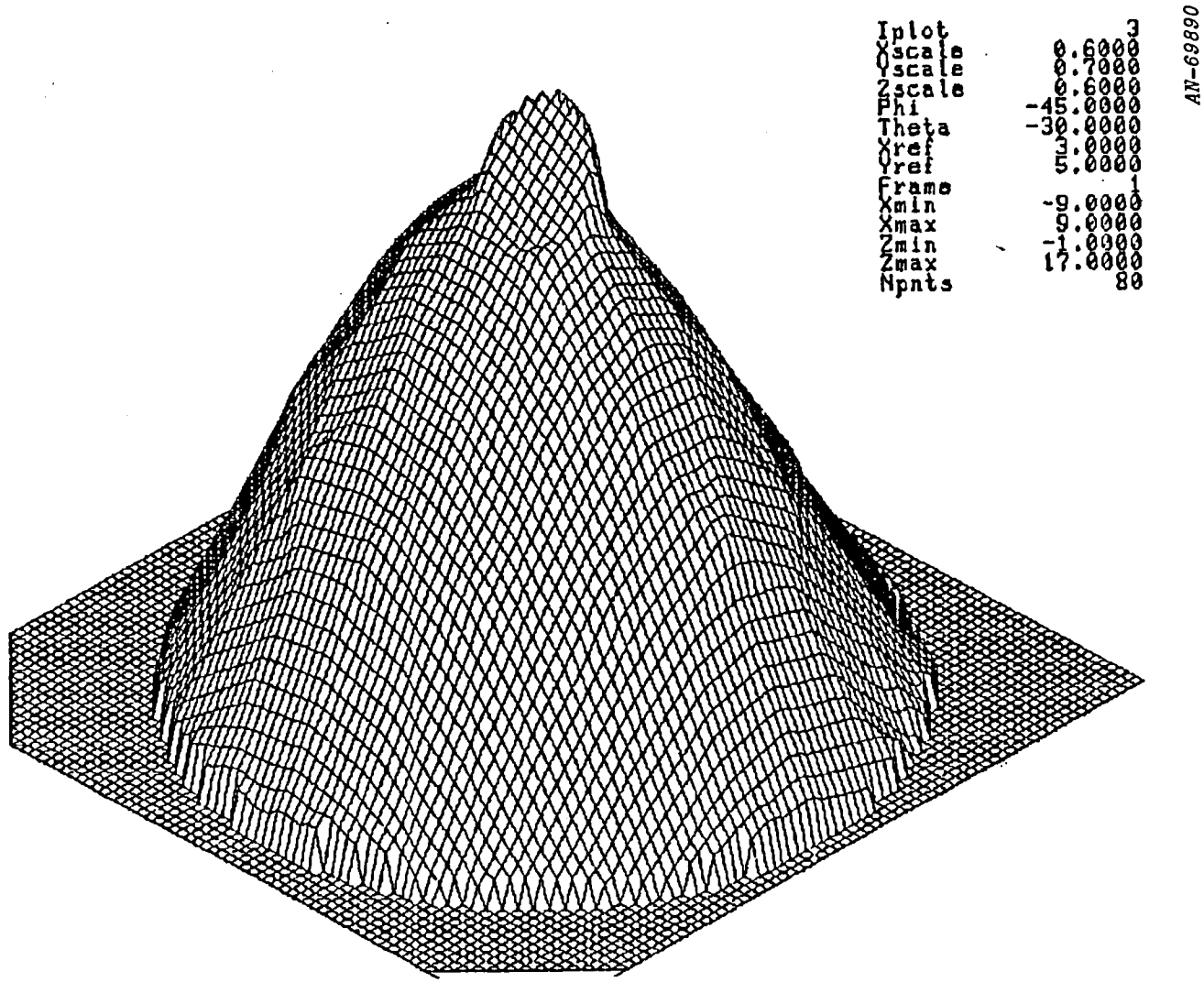

Figure 3.9 Measured Reflector Shape From Test GOS60

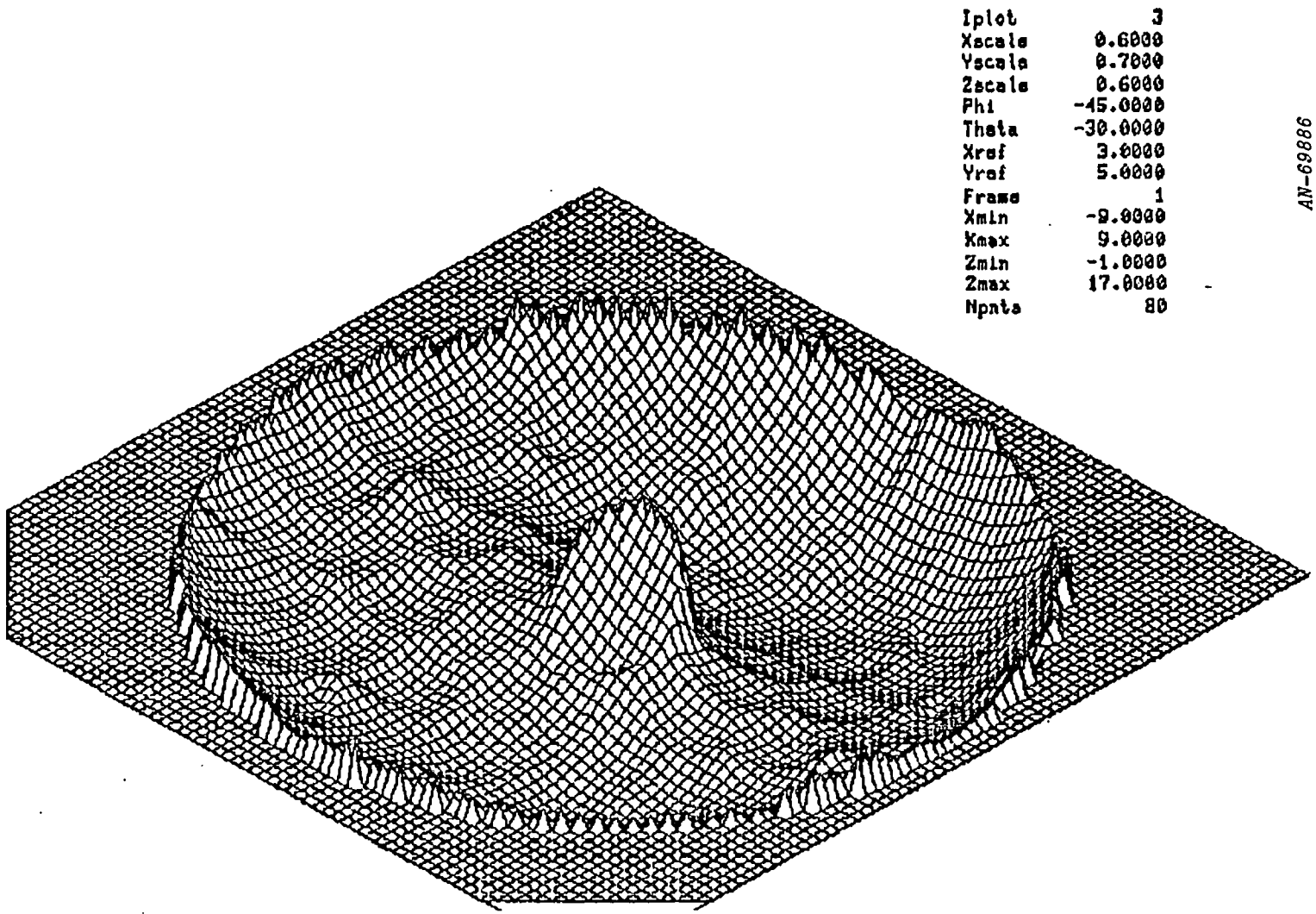

Figure 3.10 Surface Error Distribution for Test GOS60
(Ideal Curvature = 11.96 m)

Table 3.5

SUMMARY OF MEASURED TEST RESULTS

Test	ΔZ (cm)	f_m	ρ (m)	Z_m (cm)	σ_z (cm)
Ideal	30.99	1.0	9.75	0.15	0.10
GOS100	28.26	1.09	10.65	2.55	1.13
GOS80	26.38	1.17	11.4	2.66	1.15
GOS60	25.13	1.23	11.96	3.1	1.28

4 UNDERSTANDING THE TEST DATA

Two major design flaws are apparent from the test data. The overall reflector shape is much closer to a conical surface than a sphere and a large number of azimuthal wrinkles exist in the reflector photographs. Both deficiencies are major figure errors which require correction before one may rate the design successful.

Several activities were undertaken to help with the understanding of the test data. The test data was compared to analytic data which could identify the stress state of the configuration. Also, tests using coupon samples of Tedlar film were made at GRC. The tests included uniaxial and constant stress tests on Tedlar with various edge conditions. It is apparent from these materials tests that quality control improvements need to be undertaken in the fabrication of the membrane reflector. It would also be beneficial to eliminate catenaries or undertake a rigorous catenary design analysis. These design recommendations will be given next. Thereafter, the rationale for the recommendations will be provided.

4.1 DESIGN RECOMMENDATIONS

Improved Preformed Shape. The joining of twelve gore elements into the preformed spherical surface with twelve faces needs to be performed more accurately. The preformed surface currently has errors up to 2.8 cm (1.2 in). The ratio of aperture diameter to surface departure (or error) is an important index of the fabrication requirements. An accuracy of 488 cm/0.1 cm or 4800 was needed for a successful test. The fabricated surface had an index of 488 cm/2.8 cm or 174 which is not very good. Electrostatic pressure is able to provide high-fidelity shape corrections up to about $\pm$0.2 cm for this model. (The available field strength limits the correction forces or mechanical stroke that can be achieved). Thus, the preformed shape errors of 2.8 cm are 14 times larger than the available stroke of the actuators. Improvements must be made in quality control.

Membrane reflector quality could be improved by several actions. First, the shape of each gore panel that NASA is using should be compared with the gore shapes predicted in Sec. 5. (NASA indicated that their pattern is different.)

Second, a master mold should be fabricated which would be used during the splicing together of the panels. A master mold of the entire surface would certainly aid in realizing the membrane fabrication accuracy of 4800. A complete master mold would aid in lay-up of the seams as well as the catenaries. Lack of master mold is also probably responsible for the many small-scale wrinkles. Master mold replication would go a long way toward minimizing the fabrication errors noted in the test data.

Improved Catenaries. The woven Dacron (80 lb test fishing string) used in the catenaries is much too elastic. A much more inelastic cord is needed. The original design specified the use of a 2500 lb tensile strength uniaxial Kevlar or graphite fiber, which would have provided a very inelastic boundary restraint.

NASA's approach to the catenary requirement was to use a thin elastic cord and apply a significant pre-tension to the cord before testing with electrostatics. This cord was located inside a thin tube that was bonded to the membrane. Because the elastic cord required a high tension, it would alter the shape of the preformed surface from spherical toward a conical geometry. This catenary design was incompatible with GRC's design goals of maintaining an untensioned membrane with a specified spherical shape. An inelastic cord is required along the edge of the membrane. It should be bonded directly to the membrane. The precision lamination of these inelastic fibers would be aided by a catenary template and the master mold for the membrane. A stiff catenary would substantially reduce the numerous azimuthal wrinkles. Azimuthal wrinkles did not develop on the f_N 3.5

reflector because of the inelastic perimeter constraint. In retrospect, it might have been better to have first specified a rigid mount for this f_N 1.0 configuration rather than attempting the more adventurous design with catenaries. Experience in designing and fabricating the catenaries should probably resort back to smaller models. Only after experience gained by fabricating smaller catenaries at NASA should the more complex catenary scheme have been introduced.

Alignment Techniques. Testing and alignment of the EMR in the vertical plane (boresight horizontal) has caused difficulties. The effect of gravity makes alignment of the preformed membrane difficult in this position. At each of the 12 catenary apex locations are the three position adjustments. The radial adjustment is the most significant because it influences the overall tension in the catenary as well as influencing the radial shape of the preformed membrane. A pre-load should not be applied to the catenary that would stress the membrane. Rather, the catenary should be tensioned by the application of pressure to the membrane reflector.

A noteworthy approach initiated by NASA to align the EMR would incorporate load cells at each apex. During high voltage operation, the load cells would be monitored and apex position adjustments would be made during operation. By cycling around the perimeter, the positions and stresses at each apex point could be adjusted. Load cells were made by NASA to measure the nominal 12 N (2.7 lb) at each apex during operation. Problems with the weight of each load cell prevented their use. Attempts should be made to improve the load cell design for use in the future.

Some consideration should be given to membrane alignment while in the horizontal plane rather than in the vertical. It may be easier to adjust the tension at each apex when the membrane is uniformly tensioned by gravity. The theodolite system must be relocated so measurements can

be made. With this relocation to a horizontal plane, electrostatic tests would also be performed in this orientation.

Membrane Material. The quality of Tedlar film has not matched the quality of Kapton film used with the f_N 3.5 design. The Tedlar film has a waviness in the sheet stock that appears as "roller-striations" caused either during film manufacturing or during vacuum metalization. The advantages of Tedlar all its lower hygroscopic expansion coefficient and slightly lower stiffness than Kapton. The lower stiffness is beneficial by allowing either lower operating voltages or larger deflections (stroke). The original Kapton film had a stiffness (the product of thickness times modulus of elasticity) of about 800,000 lb/in_2 x 0.0003 in = 240 lb/in. The Tedlar film has a stiffness of 400,000 lb/in^2 x 0.0005 in = 200 lb/in, by allowing larger deflections with the available electrostatic force. If a smoother Tedlar film could be obtained, it should be used again. Otherwise the Kapton should be secured.

4.2 BEHAVIOR OF TEDLAR FILM

Tests were performed on small witness-samples of Tedlar to aid in understanding the poor appearance of the f_N 1.0 test article (Fig. 2.7). The specific noted material peculiarities in tests GOS60, GOS80, and GOS100 included the following:

- Inability of the nominal electrostatic force, 2.6 N/m^2 (0.05 lb/ft^2), to eliminate both large-and small-amplitude wrinkles. The large-amplitude wrinkles were predominantly in the azimuthal direction. The small-amplitude wrinkles were present in the raw material from the vendor.

- The large change in the centerline deformation of the membrane (3.13 cm) between test GOS100 and GOS60 was an order of magnitude larger than expected.

Several simple tests were initiated at GRC to identify how surface wrinkles develop in Tedlar and to estimate the material tensile stiffness. The qualitative and quantitative data acquired on Tedlar is by no means complete. These rudimentary tests suggest refinements of these tests on Tedlar and other candidate polymer films.

Two series of tests were performed on the Tedlar witness samples. In the first, uniaxial loads were applied to the 12 x 16 cm membranes with different magnitudes of initial wrinkles. The relative attenuation of the amplitude of wrinkles was measured. The second series of tests employed a drop-tower to measure the biaxial stiffness and strength of the membrane. Data and photos from both tests will be presented subsequently. First, however, several key observations are highlighted.

In the wrinkled state of some Tedlar samples, the tensile stiffness is nonlinear. The permanent wrinkles in the membrane act as soft springs. An initial small stress produces a substantial geometric deflection. As the permanent creases and wrinkles are partially attenuated, the stiffness increases asymptotically toward the basic material stiffness. The apparent lower modulus is the principal factor causing the large centerline geometric deflections between test GOS100 and GOS60.

Large-amplitude wrinkles can develop in Tedlar when the stress is primarily uniaxial. The crests of the wrinkles are parallel to the direction of the applied stress. Thus, for the f_N 1.0 configuration, the azimuthal wrinkles indicate a predominantly azimuthal stress—i.e. the radial stress is substantially less than the azimuthal stress.

The uniformity of the boundary conditions during uniaxial tests strongly influenced the development of wrinkles parallel to the direction of the maximum stress. The boundary conditions are much less critical if a biaxial stress distribution exists--i.e. the two principal

stresses in the membrane element are about the same. This may not be the case for the f_N 1.0 model. There is a strong indication that the catenaries are relatively ineffective. Without an adequately stiff catenary, the radial stress diminishes and the azimuthal stress becomes substantially larger. The presence of azimuthal wrinkles when using the weak Dacron/Kapton catenaries should be expected.

Uniaxial Tests

Tedlar witness samples were subjected to various levels of uniaxial stress to characterize the magnitude and nature of the wrinkles. The stress magnitude of these tests bracketed the f_N 1.0 model:

centerline - 1.68 MN/m^2 (244 psi)
radial stress at catenary - 1.23 MN/m^2 (178 psi)
azimuthal stress at catenary - 0.36 MN/m^2 (53 psi)

The stresses in the uniaxial tests were from 0.22 to 1.79 MN/m^2 (32.5 to 260 psi). Besides varying the stress, the membrane was subject to different boundary conditions and severity of permanent wrinkles. Several of these results are presented in Fig. 4.1 thru 4.9.

The different surface textures of Tedlar are shown in Figs. 4.1 through 4.3. A weighted bar was used to tension the membrane to the desired stress. The periodic wrinkles in Fig. 4.1 are a consequence of the uniaxial stress and the non-ideal boundary conditions. The wrinkles in Figs. 4.2 and 4.3 are caused by tight packaging and unwrapping of the membrane. The larger-amplitude wrinkles are substantially attenuated in Fig. 4.3. The largest wrinkles in Fig. 4.3 are about 0.5 mm (0.002 in).

The quality of the Tedlar film varied considerably along the roll. A large portion of the film has high spatial frequency wrinkles. These wrinkles are sometimes denoted as "roller striations", caused either during vacuum metalization or during film manufacturing. Figures 4.4

Figure 4.1 Unwrinkled TEDLAR in Tension Displaying Uniaxial Wrinkles. Nominal stress is 0.896 NM/m^2 (130 psi)

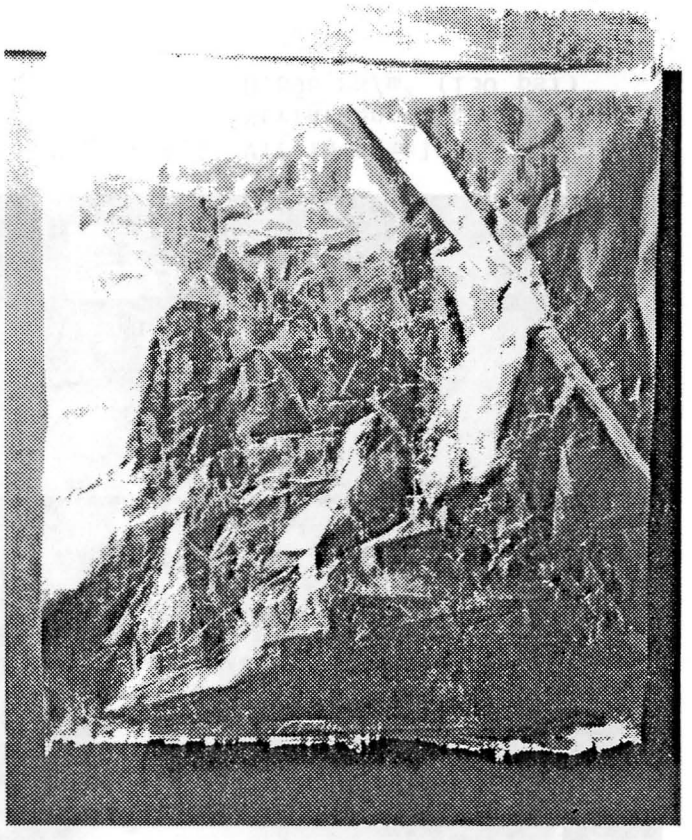

Figure 4.2 Unpackaged TEDLAR with Numerous Permanent Wrinkles. No Applied Load.

AN-70116

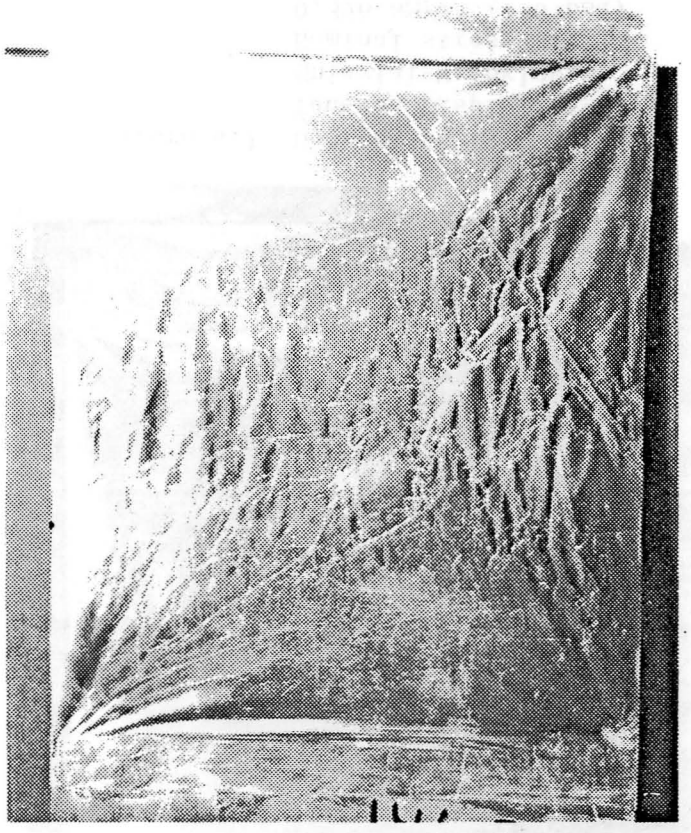

Figure 4.3 Wrinkled Tedlar Sample (Figure 4.2) but Under a Uniaxial Stress of .896 MN/M^2 (130 psi)

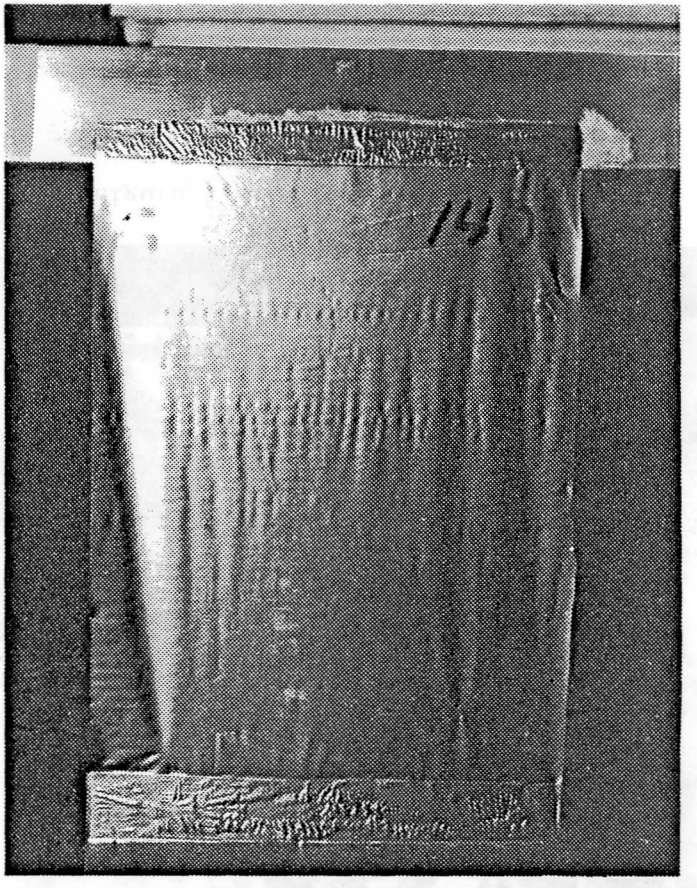

AN-70117

Figure 4.4 Virgin Sample with "Roller Striations" Stressed to 0.896 MN/m^2 (130 psi)

and 4.5 display these residual wrinkles at two stresses. The magnitude of the wrinkles is about 1.0 mm (0.040 in).

The beneficial effect of increased stress on Tedlar is summarized in Figs. 4.6 through 4.9. The samples were photographed after being stressed for an hour. Resources did not permit a measurement of the RMS roughness over the surface. A qualitative measurement of peak amplitude of the periodic wrinkles on the four samples is shown in the following table.

Uniaxial Stress, MN/m^2	Deflection (0 to P), mm
0.22	2.7
0.45	.5
0.9	.5
1.8	.5

The visual perception of the magnitude of the wrinkles tends to be exaggerated. Wrinkles are still present at the nominal operating stress but their magnitude is acceptable. The largest of these residual wrinkles are not attenuated with the unaxial loading. Future biaxial tests would be very useful for determining the residual roughness.

Stiffness Tests

A dropweight impact system was employed to obtain the mechanical properties of several membranes. The instrumented drop weight impacts the center of a 12.7 cm (5 inch) circular membrane clamped along the perimeter. Force and acceleration data from the drop weight are recorded automatically in a digitized format. This system, known as Dynatup incorporates a central data processor and graphics printer. Figures 4.10 and 4.11 compare the load and energy deformation profiles for Kapton and Tedlar. The tabulated results below the plots include critical time, load, and energy values which are results of the unit's central data processor analysis. Both samples were tested to failure.

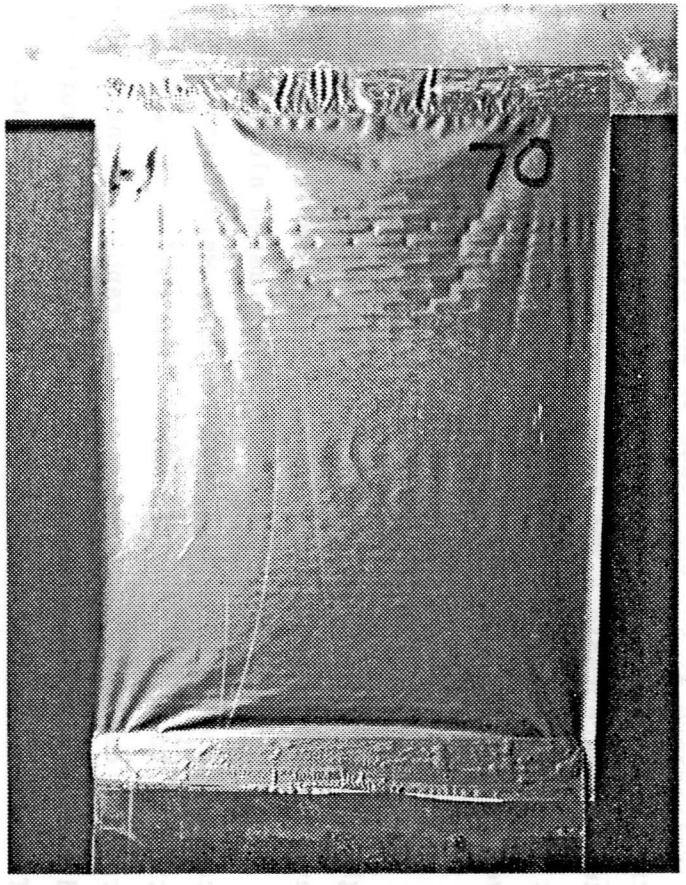

Figure 4.5 Virgin Sample with "Roller Striations" Stressed to 0.448 MN/m^2 (65 psi)

Figure 4.6 Tedlar tensioned to 0.22 MN/m^2 (32.5 psi)

AN-70118

Figure 4.7 Tedlar Tensioned to 0.448 MN/m^2 (65 psi)

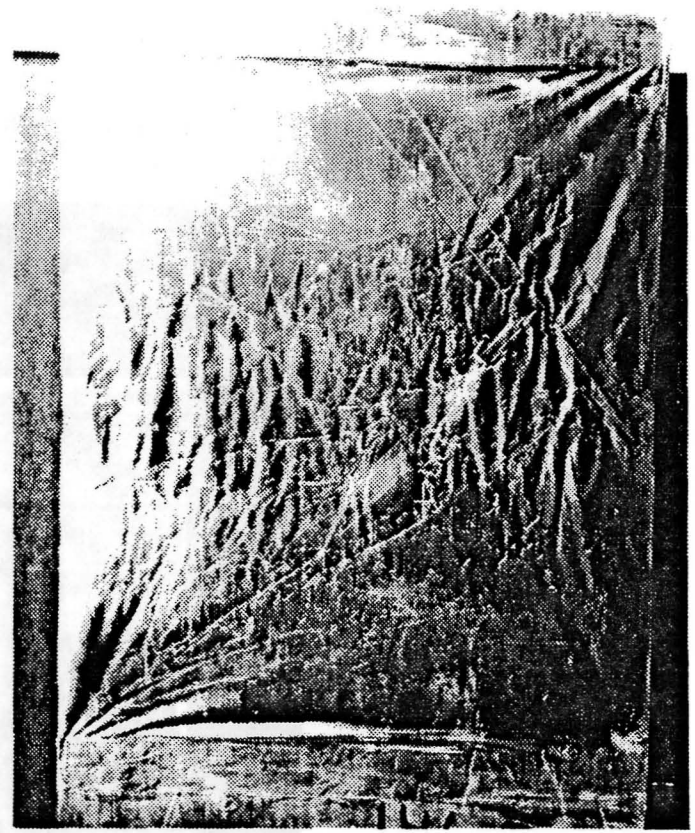

Figure 4.8 Tedlar Tensioned to 0.896 MN/m^2 (130 psi)

AN-70119

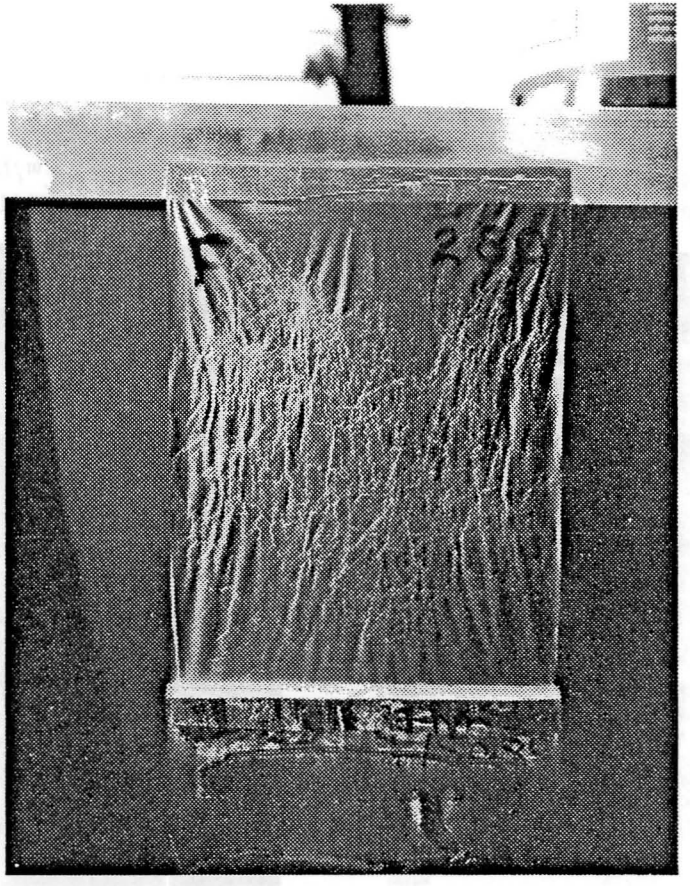

AN-70120

Figure 4.9 TEDLAR tensioned to 1.79 MN/m^2 (260psi)

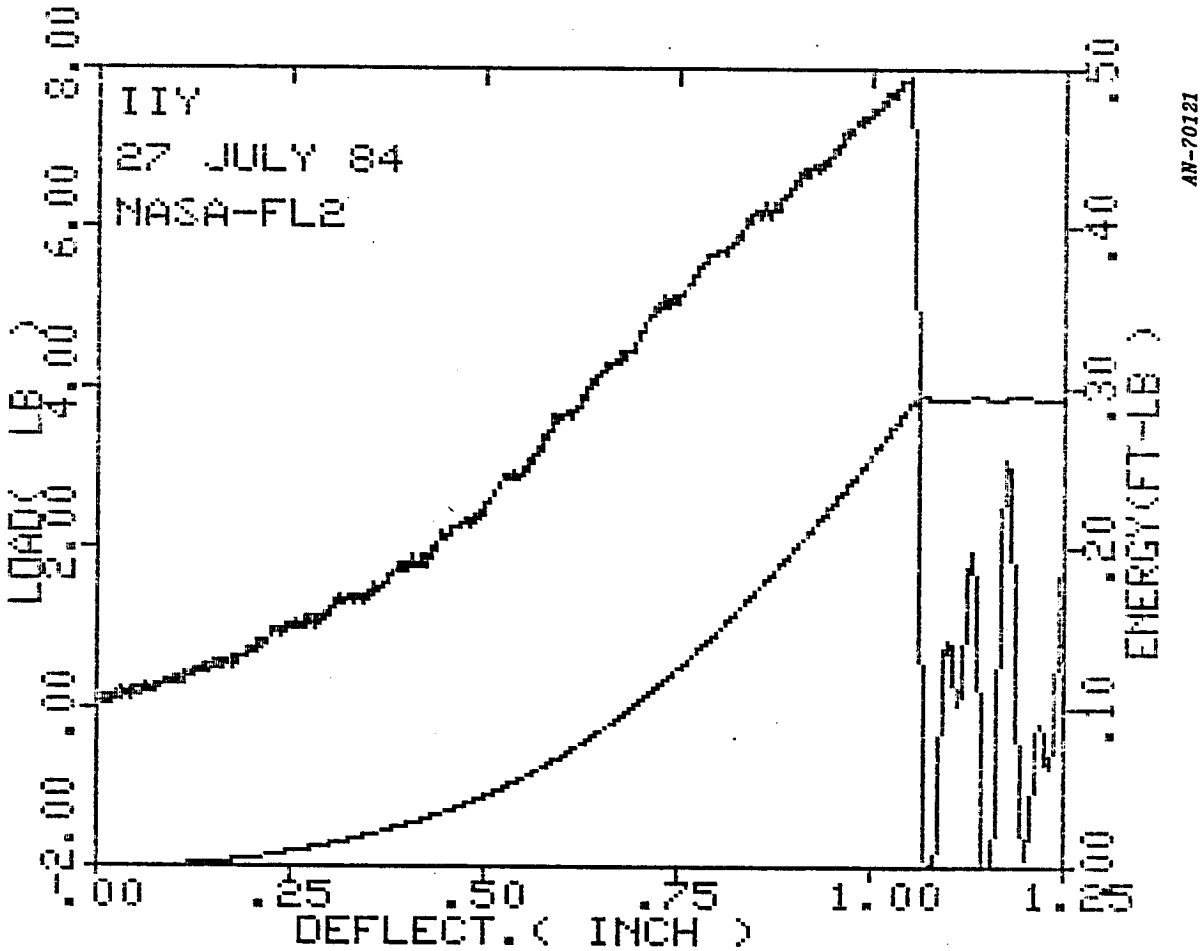

IMPACT

SPECIMEN ID/ TEMP (F)	ENERGY (FT-LB)/ SLOPE (LB/IN)	VELOCITY (FT/SEC)	LOAD (LB)/ TIME(MSEC) YIELD	MAX LOAD	MAX E	ENERGY(FT-LB)/ YIELD	MAX LOAD	DEFLECTION(INCH) PROP	MAX E
NASA-FL2		14.09	0.00	7.91		0.00	.29	.01	.30
75.00	.000E+01	11.52	0.00	7.54	7.69	0.00	1.05		1.07

FILTER NO.= 1

NO SMOOTHING.

Figure 4.10 Load-Deflection for 0.5 mil Tedlar

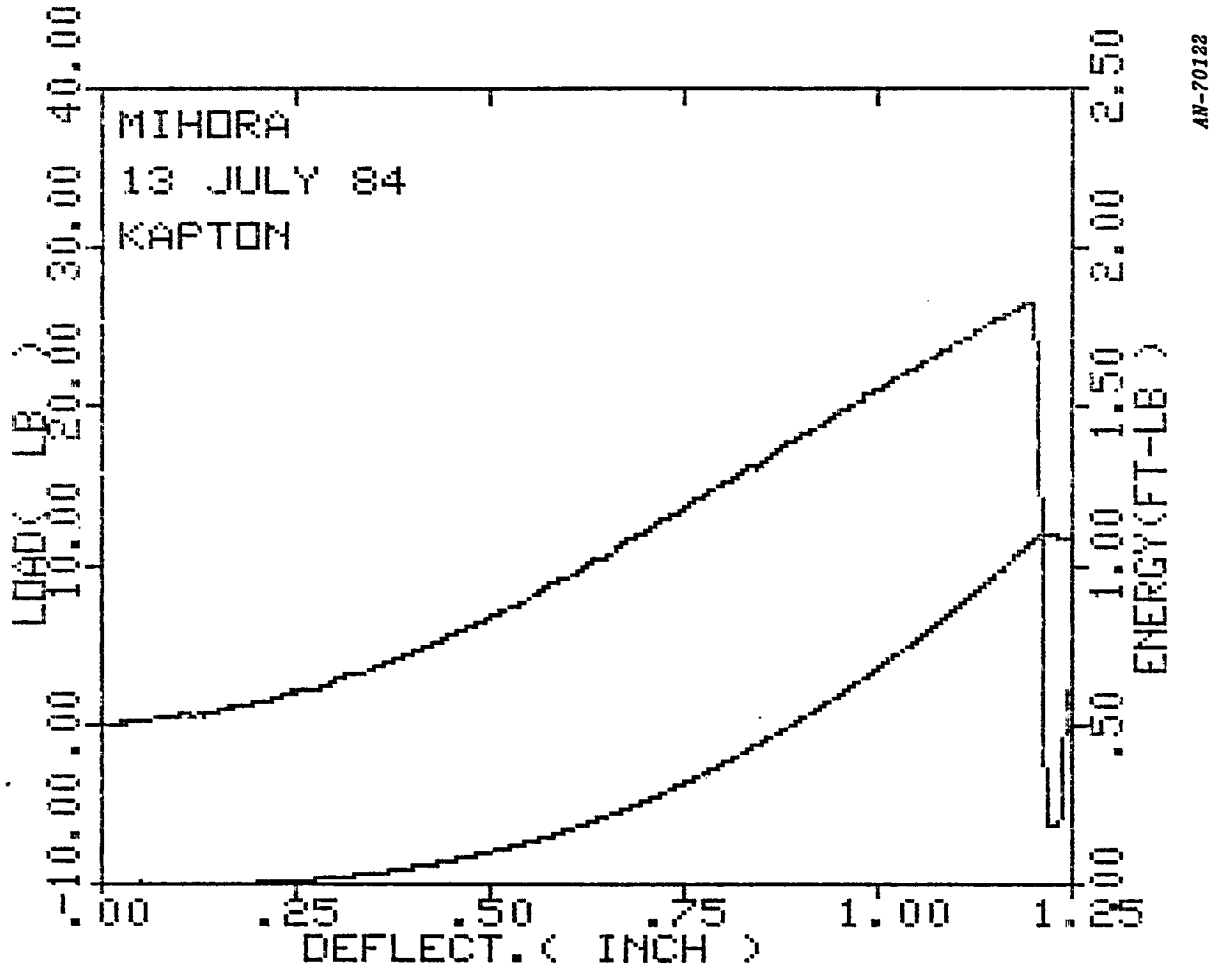

IMPACT

SPECIMEN ID/ TEMP (F)	ENERGY (FT-LB)/ SLOPE (LB/IN)	VELOCITY (FT/SEC)	LOAD (LB)/ TIME(MSEC) YIELD	MAX LOAD	MAX E	ENERGY(FT-LB)/ DEFLECTION(INCH) YIELD	MAX LOAD	PROP	MAX E
KAPTON		14.35	20.92	26.73		1.08	1.08	.03	1.11
75.00	.174E+02	11.63	8.58	8.58	8.72	1.20	1.20		1.22

FILTER NO.= 1

NO SMOOTHING.

Figure 4.11 Load-Deflection for 0.5 mil Kapton

The 1.0 inch diameter spherical indenter produced large plastic deformation into both samples before failure. Wrinkles were not present in the test samples. The results indicate that Kapton is stiffer and stronger than Tedlar.

5 GEOMETRY OF PREFORMED MEMBRANE REFLECTOR

The original requirement[1] for the membrane reflector identified a preformed spherical surface with a radius of curvature of 9.86 m. Fabrication details were left to NASA because of their prior experience in fabricating spherical meteorological balloons. Several general guidelines to NASA included the use of catenaries and 12 gore panels for the lay-up. NASA used an in-house computer program to calculate the gore pattern. Because of questions about the accuracy of the final preformed shape, an independent derivation of the gore geometry was accomplished. The derived gore pattern is slightly different than the NASA gore pattern. The derivation of the gore pattern is presented next.

Because of the lack of doubly curved membrane elements, a twelve-sided surface of singly curved panels is proposed for the $f_n = 1.0$ EMR. Figure 5.1 illustrates the design using twelve identical panels fabricated from flat membrane film. In the azimuthal direction, the membrane surface is flat--i.e. one of two principal radii of curvature is infinite. Along the seam lines, the other principal radius of curvature is specified as 9.86 m. Upon the application of electrostatic force, the radius of curvature in the azimuthal direction will decrease, approaching the radius of curvature in the radial direction. Some billowing between seams will be present with the electrostatic force. The following analysis determines the geometry of a gore that would be cut from flat sheet stock.

The coordinate variables defining the pattern for a single gore element are shown in Fig. 5.2. The problem is to determine the gore

---

[1] D.J. Mihora, Preliminary Design Notes on a Low F-Number EMR, NASA CR-165953, May 1982.

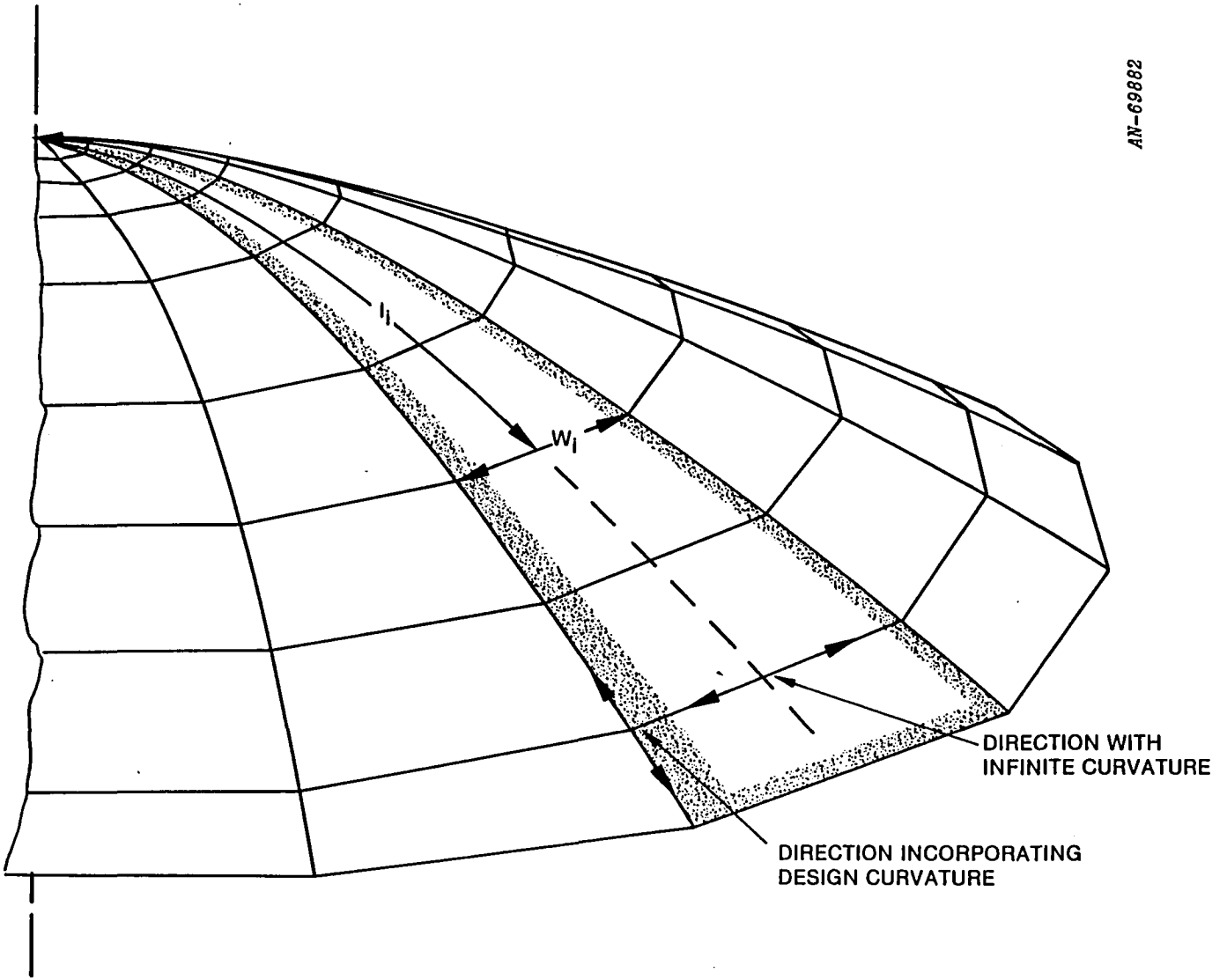

Figure 5.1 Construction of Spherical Surface Using
Flat Membrane Panels

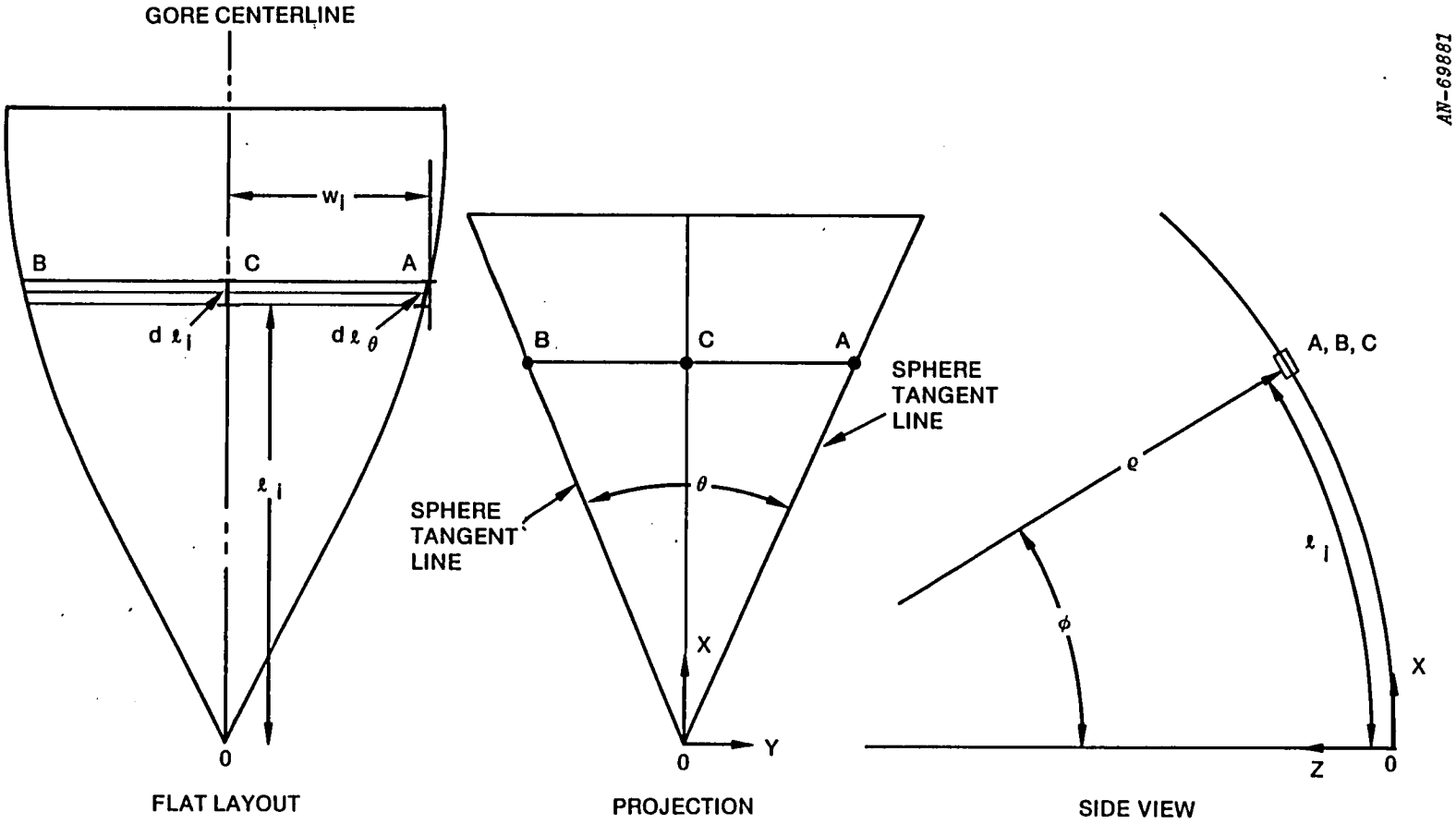

Figure 5.2. Coordinates for a Single Gore Element

both methods predict the same gore pattern to four significant figures, which is probably better than the available fabrication accuracy.

Exact Solution

The coordinates for a single gore element (the shaded panel in Figure 5.1) are shown in Figure 5.2. The gore panel has a constant curvature, shown in the x-z plane. The distance w_i is a straight line while the distance ℓ_i is an arc length. Figure 5.3 is an expansion of the differential element which has length w_i and infinitesimal width, $d\ell_i$.

The centerline arc-length ℓ_i is

$$\ell_i = \int_0^{C_x} \left(1 + \left(\frac{dz}{dx}\right)^2\right)^{\frac{1}{2}} dx \tag{1}$$

The derivative $\frac{dz}{dx}$ is obtained subsequently. The following identities are noted:

$$A_x = C_x \tag{2}$$

$$A_z = C_z \tag{3}$$

$$A_y = A_x \tan \theta/2 \tag{4}$$

The spherical surface is tangent to the gore seamline through the lines: O-A and O-B. The spherical surface is

$$A_x^2 + A_y^2 + (A_z - \rho)^2 = \rho^2 \tag{5}$$

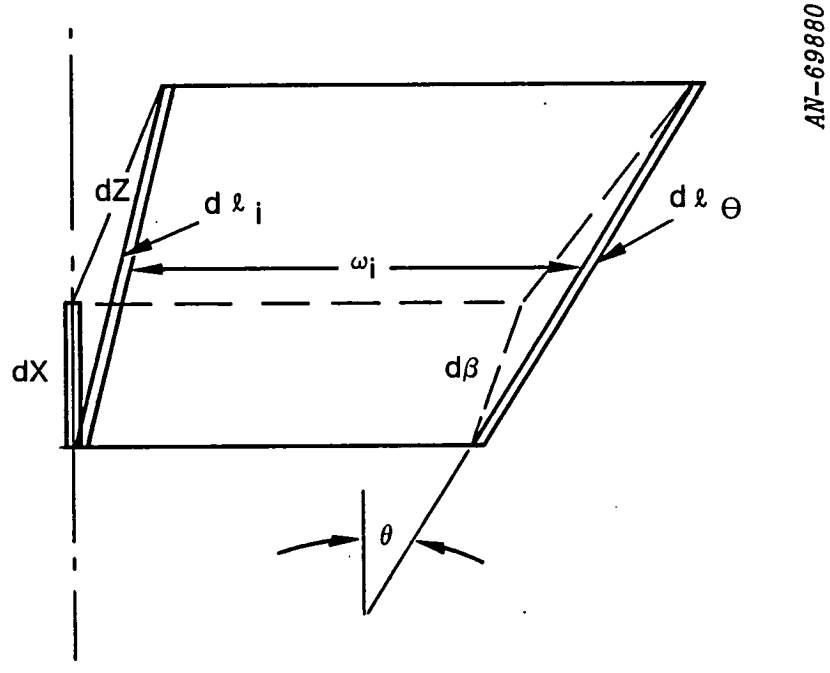

Figure 5.3 Differential Element on the Gore Face
(to be used only with the approximate solution)

From geometry, it can be shown that

$$A_z = A_x \sqrt{1 + \tan^2\theta/2} \quad \tan \phi/2 \tag{6}$$

Combining the previous two equations, one obtains:

$$C_x = x = 2\rho(z/x)/[1 + \tan^2\theta/2 + (z/x)^2] \tag{7}$$

Taking differentials of the previous equation yields

$$\frac{dz}{dx} = \frac{x(1 + \tan^2\theta/2)}{\rho - z} \tag{8}$$

Substituting into the first equation, the arc-length becomes:

$$\ell_i = \int^{C_x} \left(\frac{1 - ax^2}{1 - bx^2}\right)^{\frac{1}{2}} dx \tag{9}$$

where $a = b(1 - t)$

$b = t/\rho^2$

$t = 1 + \tan^2 \theta/2$

This integral is an elliptic integral of the second kind and requires a simple numerical solution. A Simpson Integration was used of the form

$$\ell_i = (f_o + 4f_1 + 2f_2 + \ldots . 4f_{n-1} + f_N)h/3$$

with $h = (x_n - x_o)/n$

The gore half width at this distance is simply:

$$w_i = A_y = C_x \tan \theta/2 \tag{10}$$

Approximate Solution

An approximate functional solution can be derived with the aid of Fig. 5.3. The differential element in Fig. 5.3 is w_i in width and incrementally long $d\ell_i$. For this element, the following geometric relations are noted:

$$dx = d\beta \cos \theta \tag{11}$$

$$dx = \sqrt{d\ell_i^2 - dz^2} \tag{12}$$

$$d\beta = \sqrt{d\ell_\theta^2 - dz^2} \tag{13}$$

Combining Eqs. 11-13 and rearranging, one obtains:

$$d\ell_i = d\ell_\theta \sqrt{\cos^2\theta + (1 - \cos^2\theta)\left(\frac{dz}{d\ell_\theta}^2\right)} \tag{14}$$

For the reflector geometries of interest, the $\frac{dz}{d\ell_\theta}$ and θ terms are small and Eq. 14 can be simplified to

$$d\ell_i = \cos\theta \, d\ell_\theta \tag{15}$$

Since a sphere is tangent to line O-A, the arc length of the gore edge is

$$\ell_\theta = \rho\phi$$

and the centerline arc-length is

$$\ell_i = \rho\phi \cos\theta \tag{16}$$

The gore width as a function of centerline arc length is

$$w_i = R_i \sin \theta \tag{17}$$

where $R_i = \rho \sin \phi_i$

Combining Eqs. 16 and 17 yields

$$w_i = \rho \sin \theta \sin [\ell_i / (\rho \cos \theta] \qquad (18)$$

Table 5.1 lists a BASIC program to compute the "exact" pattern by Simpson's rule. Table 5.2 compares the results between the exact solution (Eqs. 9, 10) and the approximate solution (Eqs. 16, 18). The parameters for the gore area following:

- radius of curvature, $\rho = 384$ in
- half gore angle, $\theta = 15^o$

The results in Table 5.2 provide a convincing argument that the gore geometry is properly calculated. Also, the simplified solution given by Eq. 18 is quite acceptable for the geometries being used.

Table 5.1

BASIC PROGRAM TO DETERMINE GORE PATTERN

```
2640    REM NASA GORE SHAPE
2650    DEG
2660    INPUT "CURVATURE, INCHES  ";RHO
2670    INPUT "GORE ANGLE, DEG  ";THETA
2680    INPUT "APERTURE RADIUS  ";R
2690    INPUT "PRINTOUTS ";INC
2700    REM
2705    PI=3.141592653589793
2706    RAD=PI/180
2710    AZ=RHO-SQR(RHO^2-R^2)
2720    PHI=2*ATN(AZ/R)
2730    DPHI=PHI/INC
2740    T=1.+(TAN(RAD*THETA/2))^2
2750    B=T/RHO^2
2760    A=B*(1-T)
2770    REM
2780    FOR J=1 TO INC
2790    PHII=J*DPHI
2800    TP=TAN(PHII/2)
2820    CX=(2*RHO*TP*SQR(T))/(T*(1+TP^2))
2830    LAC=CX*TAN(RAD*THETA/2)
2840    REM SIMPSONS INTEGRATION NJ WITH INCREMENTS OF 2
2850    NJ=10*J
2860    H=CX/NJ
2870    SUM=0
2880    FOR JK=0 TO NJ
2890    IF JK=0 THEN COEF=1:GOTO 2920
2900    IF JK=NJ THEN COEF=1:GOTO 2920
2910    IF JK=INT(JK/2) THEN COEF=2:GOTO 29290 ELSE COEF=4 :GOTO 2920
2920    XD=JK/NJ*CX
2930    XPHI=JK/NJ*PHII
2940    G=SQR((1-A*XD^2)/(1-B*XD^2)
2950    SUM=SUM+COEF*G
2960    NEXT JK
2970    LOC=H*SUM/3
2980    PRINT "CENTERLINE    LATERAL"
2990    PRINT USING "###.##       ";LOC,LAC
3000    AY=CX*TAN(RAD*THETA/2)
3010    XR=SQR(CX^2+AY^2)
3020    XAZ=RHO-SQR(RHO^2-AY^2-CX^2)
3030    PRINT "RADIUS         VERTICAL"
3040    PRINT USING "###.##       ";XR,XAZ
3050    NEXT J
3060    END
```

Table 5.2

COMPARISON OF GORE GEOMETRY USING TWO TECHNIQUES

Increment J	Seam Radius R (XR)	Seam Height Z (XAZ)	Centerline (Eqn 9) ℓ_i (LOC)	Exact (Eqn 10) w_i (LAC)	Approximate (Eqn 18) w_i
1	10.12	0.13	9.77	2.62	2.62
2	20.22	0.53	19.54	5.23	5.23
3	30.32	1.20	29.32	7.85	7.85
4	40.39	2.13	39.09	10.45	10.44
5	50.44	3.33	48.87	13.05	13.06
6	60.45	4.79	58.65	15.64	15.64
7	70.42	6.51	68.43	18.22	18.23
8	80.43	8.50	78.22	20.79	20.80
9	90.20	10.74	88.01	23.35	23.36
10	100.00	13.25	97.80	25.88	25.90

1. Report No.	2. Government Accession No.	3. Recipient's Catalog No.
NASA CR-172477		

4. Title and Subtitle	5. Report Date
DATA APPENDIX : F-NUMBER = 1.0 EMR WITH A FLEXIBLE BACK ELECTRODE	2 Aug 1984
	6. Performing Organization Code
7. Author(s)	8. Performing Organization Report No.
D. J. Mihora	GRC-CR-4-998
	10. Work Unit No.
9. Performing Organization Name and Address	11. Contract or Grant No.
General Research Corporation P.O. Box 6770 Santa Barbara, CA 93160-6770	13. Type of Report and Period Covered
12. Sponsoring Agency Name and Address	Contractor report
NASA Langley Research Center Hampton, VA 23665	14. Sponsoring Agency Code

15. Supplementary Notes

Langley Technical Monitor: J. W. Goslee

16. Abstract

Test data acquired from a NASA Langley Research Center fabricated reflector antenna was analyzed to better understand its performance. The antenna, a low f-number Electrostatic Membrane Reflector (EMR) incorporated a preformed membrane reflector surface as well as a preformed electrode control surface. NASA selected the polymer material and geometry for the membrane reflector surface discussed in this report. The overall reflector shape was much closer to a conical surface than a sphere and unfortunately, the limitations of the mechanical stroke of the model prevented improvement in shape to the desired f_n=1.0 spherical aperture. Design improvements include proper gore shape and perimeter catenary.

17. Key Words (Suggested by Author(s))	18. Distribution Statement
Membrane Electrostatic Active Control	

19. Security Classif. (of this report)	20. Security Classif. (of this page)	21. No. of Pages	22. Price
Unclassified	Unclassified	67	

For sale by the National Technical Information Service, Springfield, Virginia 22161